

A KINEMATIC AND KINETIC ANALYSIS OF A FROG LAUNCHING FROM
WATER USING DIGITAL PARTICLE IMAGE VELOCIMETRY

By Kit C. Wilkinson

A Thesis

Submitted in Partial Fulfillment
of the Requirements for the degree of
Master of Science
in Biology

Northern Arizona University

December 2014

Approved:

Kiisa Nishikawa Ph.D. Chair

Brent Nelson Ph.D.

Stan Lindstedt Ph.D.

Theodore Uyeno Ph.D.

UMI Number: 1571873

All rights reserved

INFORMATION TO ALL USERS

The quality of this reproduction is dependent upon the quality of the copy submitted.

In the unlikely event that the author did not send a complete manuscript and there are missing pages, these will be noted. Also, if material had to be removed, a note will indicate the deletion.



UMI 1571873

Published by ProQuest LLC (2014). Copyright in the Dissertation held by the Author.

Microform Edition © ProQuest LLC.

All rights reserved. This work is protected against unauthorized copying under Title 17, United States Code



ProQuest LLC.
789 East Eisenhower Parkway
P.O. Box 1346
Ann Arbor, MI 48106 - 1346

ABSTRACT

A KINEMATIC AND KINETIC ANALYSIS OF A FROG LAUNCHING FROM WATER USING DIGITAL PARTICLE IMAGE VELOCIMETRY

KIT C. WILKINSON

Locomoting from one medium to another is crucial to the survival of many animals. Bullfrogs (*Lithobates catesbeianus*) leap from water into air to capture aerial prey or to escape water-filled depressions. Here, kinematics and kinetics of leaping on land and water are described and compared. High-speed videography was used to record both types of leaps and these videos were analyzed for their kinematics (joint extension, duration, and take-off velocity) and to calculate kinetic energy at takeoff. A custom digital particle image velocimetry (DPIV) instrument recorded the vortex ring shed from each frog foot. Joint extension sequences of both types of leaps and differences in take-off velocities were statistically identical. The kinetic energy contained in the two vortices shed from each foot was small in magnitude compared to the kinetic energy in the body of the frog. This suggests that the kinetic energy transfer from the movement of the frog is more to other types of waves, and less to the vortices. How these frogs are able to produce enough thrust to leave the water is likely due to the paddle-like shape of their feet, their elastic, energy storing tendons and muscle fascia, powerful muscle contractions resulting in a land leap applied in water.

ACKNOWLEDGEMENTS

In the spring of 2010, Kiisa Nishikawa and Theodore Uyeno approved my admission to Northern Arizona University, a moment which changed my life for the better. They both have been there for me during some of the greatest challenges I have experienced. I truly thank you both for all the time, energy and advice you have given me.

There are many people I would like to thank for all their help with frogs, lasers, and keeping my spirit alive: Clint Barnes, Brian Burt, Andrea Bowie, Rene Fuqua, Nicholas Gengler, Alice Gibb, Glazier family, Tom Greene, Leslie Hempleman, Mike Isaacs, Daniel Kmack, David Lee, Stan Lindstedt, Ian MacDonald, Shane Meehan, Jenna Monroy, Lexi Moore, Kirstin Olmon, Sandra Nauwelaerts, Russell Nelson, Brent Nelson, Scott Nichols, Cinnamon Pace, Krysta Powers, Rosemary Rudy, Ryan Schroeder, Singne Slayton, Kamala Smith, Mr. Sylvatica, Roy St. Laurent, Uzma Tahir, Antonia Tallante, William Thielicke, Uyeno family, Kim Vercauteren-Griffin, Merrill Webb, Tom White, Max Wheeler, Weaver family, and the Wilkinson family.

I would like to especially thank Duane Barbano for your faith and confidence in me, Emma Benenati for always being willing to help me in times of need, the Cagle family for accepting me as a family member and appointing me as Liam's Godfather, Erik Dillingham for all your shenanigans and nonsense conversations while programming, Amaris Fuller for loving and being kind to me, and Kari Taylor-Burt for caring for me as my true friend.

This work could not have been performed without my best dog friend, Mr. Pippins. You have taught me more about unconditional love than anyone. Thank you Pip.

TABLE OF CONTENTS

List of Tables	vii
List of Figures	viii
Preface	x
Chapter 1. Introduction	1
References	4
Chapter 2. An economic and open-source digital particle image velocimetry instrument for measuring liquids	5
Abstract	5
Introduction	6
Materials & Methods	7
Experimental DPIV Physical Configuration	7
Flow production and flow tracing particles.....	8
Illumination system.....	9
Image Acquisition.....	10

Validation.....	10
Measure of Volume.....	11
Measure of Velocity.....	11
Software Settings.....	12
Statistical Test.....	13
Results.....	14
Volume Results.....	14
Velocity Results.....	14
Discussion.....	14
References.....	18
Chapter 3. Ballistic locomotion between media: A kinematic and kinetic analysis of a frog launching from water.....	24
Abstract.....	24
Introduction.....	25
Materials & Methods.....	27
Animals.....	27

The Kinematics of Land Leaping.....	28
The Kinematics of Water Leaping.....	29
The Kinetics of Land Leaping.....	30
The Kinetics of Water Leaping.....	31
The Vortex Kinetics.....	31
DPIV Methods.....	33
The <i>Ex-vivo</i> foot.....	36
Results.....	39
Morphometrics.....	39
The Land Leap Kinematics.....	39
The Water Leap Kinematics.....	40
The Land Leap Kinetics.....	41
The Water Leap Kinetics.....	41
The Vortex Kinetics.....	41
Discussion.....	42
References.....	46
Chapter 4. Conclusions.....	54
References.....	59

LIST OF TABLES

Table 2.1: Velocity and volume measurements from a cross-sectional area of a vortex ring using digital particle image velocimetry. The experimental statistics and associated P-values were derived by comparing the observed means to the expected means using Pearson’s chi-square test.....	19
Table 3.1: A comparison of land and water leaps in terms of the joint extension times from the beginning of the propulsion, the joint extension and propulsion duration, the take-off velocity (V_{to}), the maximum toe tip velocity, and the total kinetic energy.....	49

LIST OF FIGURES

Figure 2.1: The hardware used to construct the DPIV instrument and the components used to test the error.....	20
Figure 2.2: Wiring and circuit schematics for the Arduino Uno used to synchronize the lasers and power source from the high-speed camera's output signal.....	21
Figure 2.3: The code for the program 'Laser Fire' used to synchronize the laser pulse with the high-speed camera's output TTL signal using the Arduino Uno microprocessor.....	22
Figure 2.4: A diagram (a) of a vortex ring with the core diameter (D); the 6 radii ($r1 - r6$) were averaged and used to calculate the volume of the vortex rings. A real vortex ring (b) was measured using DPIV software and the same method.....	23
Figure 3.1: An illustration of the DPIV instrument with labeled components.....	50
Figure 3.2: Cross section of a real vortex ring in PIVlab 1.3 (a). A 3-D rendering of the cross section of vortex ring (b).....	51
Figure 3.3: A series of images depicting the preparative phase of the water leap.....	52

Figure 3.4: Frog hindlimb joint extension start, stop, and durations and kinetic energy profiles with a pictorial comparison of land and water leaps in % of propulsion time.....53

PREFACE

This thesis is divided into four chapters. The first chapter is an introduction to chapters two and three, which are meant to be individual publications. Chapter two is a methods paper on building and using a custom digital particle image velocimetry instrument. Chapter three is a biomechanical study on a frog leaping from water into air. I plan on submitting both chapters to the Journal of Experimental Biology. Chapter four is a conclusion chapter to chapters two and three and integrates the methods of chapter one with the biomechanical study of chapter three.

For the frogs.

Chapter 1. Introduction

Traveling from one medium to another is crucial to the survival of many animals. Most vertebrates can move on land and swim in water and transition between these environments, which can help exploit new prey and avoid predators (Guinet & Bouvier, 1995, Whitfield & Blaber, 1978). Anurans swim in water and leap on land, but some have been observed to leap from water into air (Herrmann, 2006, Nauwelaerts et al. 2004). I have collected video recordings of juvenile bullfrog, *Lithobates catesbeianus* (Shaw, 1802), leaping from water into air and I inquire how these frogs are able to do so.

Frogs hindlimbs have been compared to a catapult because they store elastic energy in their hindlimb tendons and fascia and release it more or less simultaneously with hindlimb muscle contractions resulting in power amplification during a land leap. Anurans will extend their skeletal sarcomeres' operating lengths beyond most vertebrates to store an even greater amount of elastic energy (Azizi & Roberts, 2010). The control mechanisms for land leaping are attributed from groups of neurons in the brainstem that send relatively simple signals that have been called 'motor primitives' (Hart & Giszter, 2010). The signals coming from these neurons can be shuffled to produce a wide variety of movements including jumping, feeding lunges, and swimming (Hart & Giszter, 2004).

Here, kinematics and kinetics of leaping on land and water are compared to describe how water leaping in bullfrogs is achieved. Biplanar, high-speed videography was used to record movements where kinematics were calculated of both leap types; these videos were used to measure joint extension duration, and take-off velocity. Take-off velocity in water is calculated from the frame when the legs are straight to the next frame. With the known mass of the frog and take-off velocity, kinetic energy was

calculated. During water leap propulsion, the frog imparts momentum to the water. The moving water takes the form of surface and pressure waves and in vortex rings. An open-source and economical digital particle image velocimetry (DPIV) instrument was developed to measure the size and velocity of the vortex rings shed from each frog foot.

The DPIV instrument was able to record video in which the internal and external radii of a ring vortex and the velocity of the particles traveling with ring could be calculated. It was rigorously calibrated using a dual-syringe pump to inject water vortices of known volume and velocity into the DPIV tank. There were no significant differences between the syringe pump velocity settings and DPIV measurements.

Before water-to-air leaps, positional movements of the frogs fore and hindlimbs interfered with visualization of vortices shed during the leap. A solution to this problem was attaching an excised foot from the frog to a servomotor. The motor moved the foot at nearly the same velocity as the live foot to produce a similar vortex in a DPIV aquarium. From DPIV data, the kinetic energy of the feet that transferred to the vortices was calculated.

I found that the hindlimb joint extension sequences of both leap types were the same, which is not what was seen in swimming frogs (Nauwelaerts et al. 2005). The kinetic energies of the frogs' bodies of both leap types did not differ, however a comparison of the total kinetic energy of the vortices shed from the feet was a small fraction to the frogs' bodies.

The bullfrog can leap from water into air. It has been suggested that the foot shape contributes in achieving this locomotion (Nauwelaerts et al. 2004). Because hindlimb

joint extension sequences are the same for both leap types, I reason that the power amplification of the hindlimb in conjunction with the foot shape results in a water leap.

References

- Azizi, E., & Roberts, T. J. (2010). Muscle performance during frog leaping: influence of elasticity on muscle operating lengths. *Proceedings of the Royal Society*, 277, 1523-1530.
- Guinet, C., & Bouvier, J. (1995). Development of intentional stranding hunting techniques in killer whale (*Orcinus orca*) calves at Crozet Archipelago. *Canadian Journal of Zoology*, 73(1), 27-33.
- Hart, C. B., & Giszter, S. F. (2004). Modular premotor drives and unit bursts as primitives for frog motor behaviors. *The Journal of Neuroscience*, 24(22), 5269-5282.
- Hart, C. B., & Giszter, S. F. (2010). A neural basis for motor primitives in the spinal cord. *The Journal of Neuroscience*, 30(4), 1322-1336.
- Herrmann, H. W. (2006). *Conraua goliath* (Goliath Frog) leaping in water locomotion. *Herpetological Review*, 37(2), 2006.
- Nauwelaerts, S., Scholliers, J., & Aerts, P. (2004). A functional analysis of how frogs leap out of water. *Biological Journal of the Linnean Society*, 83, 413-420.
- Nauwelaerts, S., Stamhuis, E., & Aerts, P. (2005). Swimming and leaping in a semi-aquatic frog. *Animal Biology*, 55(1), 3-15.
- Whitfield A.K. and Blaber S.J.M., 1978. Feeding ecology of piscivorous birds at Lake St Lucia, part 1: diving birds. *Ostrich*, 49, 185-198.

Chapter 2. An economic and open-source digital particle image velocimetry instrument for measuring liquids

Abstract

Digital particle image velocimetry (DPIV) is a technique that is widely used by biologists and engineers to visualize fluid flow and measure its velocity and geometry. The fluid is seeded with neutrally buoyant particles that are illuminated with a laser light sheet. The particle motions are recorded using a high-speed camera. A synchronizer circuit pulses the laser in time with the camera's frame capture rate. Individual frames are extracted from the video file and analyzed using open source PIV freeware. This software tracks each particle from frame to frame, and, with calibrated distance and known frame rate, individual particle velocities are automatically calculated. Validation of particle velocity within a moving volume was performed by adding a known volume of water at a known velocity into the DPIV instrument using a syringe pump. These known values did not differ significantly from those calculated by the software. Most commercial DPIV instruments cost tens of thousands of dollars. This paper describes a method wherein high-powered pen lasers, common desktop computers, open-source DPIV software, a fish aquarium, and hobby microprocessors are used to assemble a DPIV system to measure water flow for under \$2,000 USD.

Introduction

Visualizing liquid flow can help understand locomotion, cardiovascular function, or hydrodynamics by measuring flow velocity that can help calculate boundary layer thicknesses to flow type. Digital particle-image velocimetry (DPIV) is useful for visualizing liquid flow (Raffel et al., 2007); it uses a high-speed digital video camera to record neutrally buoyant, illuminated particle motion. The camera records changes in particle position in a plane that is illuminated with a laser light sheet. DPIV software tracks the particle movement, and combined with the known frame rate of the camera, the velocity of the particles can be calculated. Here, a simple DPIV system is described that most investigators can construct for under \$2000 USD.

Ryerson and Schwenk (2012) constructed a DPIV system to visualize air flow. The error estimate for their system was comparable to commercial systems. They also suggested that their system could be adapted to liquid, which was done for engineering purposes (Ring, B. P., et al. 2013), but not for biomechanical research. The focus of Ring's instrument was on laminar fluid flow to determine where and why energy losses are occurring in dividing flow junctions (Ring, B. P., et al. 2013). The instrument I have developed is designed to visualize water flow associated with biological phenomena, such as toroidal vortices, and calculate their velocities and other kinematic parameters. Commercial water DPIV instruments range in price from \$5,000-\$100,000 USD (Ryerson & Schwenk, 2012) and have been used by many different investigators in engineering (Kim D., Gharib, M. 2011b), and biological fields (Flammang, B. E., et al. 2011). The designs for the DPIV instrument presented here range in cost from \$800-\$2,000 USD. This system is also customizable for investigating fluid-related movements

in various applications. The cost of this system is lower due to its components: high-powered laser pointers, inexpensive micro-controllers, a fish aquarium, a common desktop computer, open-source DPIV software, and high-speed video cameras. The expensive high-speed video camera employed here had a higher frame rate capability than necessary to perform DPIV using this instrument, but relatively inexpensive cameras are now available.

The experimental DPIV was used to visualize flow from aquatic animal locomotion and flow generated by a mechanical simulation. Pliolite particles were used because they are biologically inert, neutrally buoyant, and reflect laser light well. To validate the DPIV recordings and subsequent measurements, the system was calibrated by comparing a known volume of water added to the DPIV system at a known velocity.

Materials and Methods

DPIV Physical Configuration

The experimental aquarium size was (0.41 m x 0.21 m x 0.25 m); the water was filled to 0.24 m from the bottom (Fig 2.1), which produced a thin boundary layer thickness over a flat plate for turbulent water flow up to $5 \text{ m}\cdot\text{s}^{-1}$ at $\sim 27^\circ\text{C}$. The experimental DPIV physical configuration was designed to avoid boundary layer effects on flow at $< 10 \text{ m}\cdot\text{s}^{-1}$, which was calculated using Prandtl's equation (Raffel et al., 2007).

$$\delta = 0.16Re_x^{0.85} \quad (1)$$

δ is the boundary layer thickness, Re is the Reynolds number (see below), and x is the height of the submerged vertical aquarium side. To determine the type of flow, the Reynolds number (Re) was calculated as follows.

$$Re = \frac{\rho v D}{\mu} \quad (2)$$

Re is the Reynolds number, ρ = the density of water at 27°C (997 kg·m⁻³), v is the mean velocity of the fluid (10 m·s⁻¹), D is average of the length, width, and height, and μ is the dynamic viscosity of water (8.94 x 10⁻⁴ Pa·s), which confirmed the adequate size of the DPIV aquarium. The back of the aquarium was painted black to the same level as the water, to provide a maximum contrast for the particles. On the back of the aquarium above the water level, a 0.01 m black and white grid was used as a scale. The top remained open for accessibility. This experimental construction provided an area of interest at approximately 0.1 m x 0.1 m to analyze vortex ring of a maximum diameter of 0.03 m.

Flow production and flow-tracing Particles

A reproducible water vortex ring was pumped into the DPIV aquarium by a Harvard Syringe Pump (Model 33, Instech Laboratories, Inc., Plymouth Meeting, PA, USA, accuracy = 0.35%, reproducibility = 0.1% based on examination by Instech Laboratories, Inc.). Two plastic 61 mL syringes (Monoject, Covidien Co., Mansfield, MA, USA) were filled with air and placed in the syringe pump next to the DPIV aquarium. Both syringe tips were connected to 0.1 m of clear vinyl tubing with the internal diameter of 0.0045 m (Airline Tubing, PETCO Animal Supplies, Inc., San Diego, CA, USA). The tubes leaving the syringes were connected via a brass T-junction with a tube leaving and inserted into the vortex ejection cylinder (Fig 2.1); this design allowed water to be sucked into the cylinder presenting a visible line between air and water. The cylinder was made of glass that was 0.1 m long with an internal diameter of 6.25 x 10⁻³ m and outer diameter of 7.70 x 10⁻³ m. It was inserted in the terminal section of the tubing and positioned equidistant from the left, right, front, and back sides of the

aquarium 0.01 m below the surface to minimize any boundary effects. A Buret clamp was used to hold the vortex ejection cylinder in a vertical position (not in Fig 2.1). The junctions were sealed with aquarium silicone to ensure that the system was watertight. The syringe pumps sucked water into the ejection cylinder and then ejected the water out into the aquarium producing a vortex ring.

Pliolite particles (Eliokem, Inc., Akron, OH, USA) were used to visualize water flow by flowing with the current. The biologically inert particles are composed of a near neutrally buoyant thermoplastic solid-resin with the density $1030 \text{ kg}\cdot\text{m}^{-3}$. The average particle diameter was $6 \times 10^{-5} \text{ m}$, which aided in DPIV software tracking but did not alter the water properties (Stamhuis & Videler, 1995). The required particle size was obtained by chopping the raw product in a blender, sieving through a sieve cylinder, and vibrating using a common fish aquarium air pump by placing the sieve cylinder on top. Particles smaller than $6 \times 10^{-5} \text{ m}$ were discarded. The concentration of Pliolite used was $6 \times 10^{-6} \text{ kg}\cdot\text{m}^{-3}$ of water.

Illumination System

Three green light sheets were projected by lasers composed of neodymium-doped yttrium aluminum vanadate (Wha Fat Technological Co., Ltd, Hong Kong, China, $\lambda = 532 \text{ nm}$, $P_{\text{max}} = 0.8 \text{ W}$) at right angles to each other to avoid shadows. A cylindrical lens was, carefully removed from the emission aperture of a laser level [which is used for leveling household objects (Central Machinery, Shenzhen, China, $f = 3.4 \times 10^{-3} \text{ m}$)] was mounted on each laser to create a vertical light sheet. The laser had light that was not aligned with the sheet probably due to imperfections from the emission aperture. A 0.002 m wide vertical paper aperture was placed on the sides of the aquarium to block stray

beams. This aperture maintained the laser sheet thickness throughout the beam in the aquarium, which yielded a 0.08 m x 0.08 m working section. The lasers were powered by a benchtop power supply (KIT-09774, Sparkfun Electronics, Boulder, CO, USA), which was adapted to a computer power source at 3.3 V. An electrical pulse at ten times the frame rate of the camera was synchronized with the microprocessor Arduino Uno (Smart Projects, Ivrea, Italy) using the transistor-transistor logic (TTL) signal from the high-speed camera and the power source. The pulsing frequency ensured that an image of the particle would be collected by the high speed camera and reduced interleaving effects. A custom script was written to synchronize the TTL signal to the lasers (Fig 2.3). A breadboard with a MOSFET IRF510 transistor was used to deliver the pulsed electrical currents to the lasers (Figs. 2a, 2b). This system allowed the particle illumination to be recorded using the high speed camera at 125 frames per second.

Image Acquisition

High-speed videography was employed to record the particle flow. The laser sheet perpendicular to the lateral view was recorded using a black and white, high-speed video camera (Phantom V5.1m, Vision Research, Inc., Wayne, NJ, USA) at 125 frames per second ($f \cdot s^{-1}$). The exposure time was 1/250 s. The lens was an AFD Nikkor (Nikon Corp., Tokyo, Japan, $f = 0.05$ m, $F = 1.4$); the maximum aperture was used to collect the most light, and the lens was focused on the laser sheet. The camera distance was determined by maximizing the front panel of the tank. The program used to collect and isolate the flow data was Phantom Camera Control Application (v2.41b Vision Research, Inc., Wayne, NJ, USA). Once the flow of interest sequence was identified, it was saved as a series of single-image files as .tiff, as required by the PIVlab 1.3 (Thielicke &

Stamhuis, 2012). The images acquired were used to calibrate the system and verify that the DPIV instrument's calculated measurements were reliable.

Validation

The vortex ejection cylinder was placed below the water surface with the vertical laser sheet crossing through its center. Vortex rings formed in this manner have known radii; thus, their volumes can be calculated by as follows.

$$V = 2\pi\left(\frac{D}{2}\right)r^2 \quad (3)$$

V is the volume of a vortex ring, D is the core diameter, and r is radius from a core to the outside boundary of the vortex ring. The velocity can be calculated dividing the particle displacement distance between the video frames and the frame rate (Fig 2.4).

Measure of Volume

The DPIV software includes tools for measuring a vortex ring core diameter and radius in a cross-section, which can be used to estimate the volume.

The diameter was calculated by measuring the vortex ring cross section D from one side of the core to the other. The core is defined as the center of the rotating water mass. The particles in the vortex had greater velocity than the particles of the background convection, giving a clear vortex boundary. The radius r was calculated by measuring the distance from the core to the outermost boundary of the ring. The radius r was not always equal because of minor convection currents colliding with the ring. An average of six radii from the same vortex ring core and from the core to the points on the outermost boundary was calculated and used in the above equation (Fig 2.4).

Measure of Velocity

The volume of 1 mL was determined by marking the vortex ejection cylinder 0.033 m from the opening (calculated from the inner diameter using the formula $\pi r^2 h$). The syringe pump was designed to expel liquids at a set rate. The 0.033 m distance divided by the duration of expulsion yields the velocity at which the water is expelled. The syringe pump ejected 1 mL at $0.026 \text{ m}\cdot\text{s}^{-1}$ (accuracy = 0.35%, reproducibility = 0.1% based on examination by Instech Laboratories, Inc.), which is the maximum expulsion velocity. An additional velocity programmed for the syringe pump was $0.016 \text{ m}\cdot\text{s}^{-1}$ with the same volume. Video data from ring vortices at these velocities were collected.

Software, Settings and Procedures

The PIVlab software tracks light reflected from the particles as they change position between each frame. The software calibration distance was determined from the 0.01 m^2 grid above the water. Five recordings at both the high and low velocity settings were made for a total of ten videos. The high and low velocity videos were analyzed for the maximum velocity and volume. The image series with the vortex ring was analyzed pairwise using PIVlab 1.3. The DPIV system can increase and decrease “magnification” depending on the particle concentration and the area of the flow due to a software filter. The software analysis used a rolling comparison with a filter that applied a 24×12 pixel interrogation area, which is the exact area where the vortex is located within the area of interest, for the first pass and 12×6 pixels for the second and third passes. The filter’s pixel interrogation area was determined using the ratio of the particle density to the cross-sectional area of the toroidal ring. Histogram equalization was used to enhance contrast. A high-pass filter was used to sharpen the image and remove background signals by isolating particles of light from pass to pass to cross-correlate the images. The software

was set to remove erroneous velocity vectors at over eight standard deviations from the mean. I used a PIVlab tool that smoothed data using a cubic spline interpolation by interpolating four to ten vectors in 400.

PIVlab uses planar coordinates of the vectors to measure the maximum velocity and volume. These parameters describe a vortex ring (Stamhuis and Videler, 1995). The rings were identified by PIVlab's vortex locator algorithm that searches for vectors travel in a circular motion. The core diameter and radius were measured from this fluid visualization. PIVlab offers a tool to analyze velocity magnitudes along a manually drawn line, which is referred the polyline analysis. In this analysis, the area with the largest vector arrows indicated the greatest velocity magnitude, and the line was drawn through those areas and maximal velocity magnitudes were noted.

The same initial frame for all trials was defined as the moment that the water began to move out of the vortex ejection cylinder. The vortex ring was fully developed after 0.04 s and the polyline analysis was performed. The maximal velocities were then noted.

Statistical Tests

The estimated flow velocities and volumes were compared with the known values using the Pearson's chi-squared test.

$$t_s = \frac{\bar{Y} - \mu_o}{\sigma} \quad (4)$$

t_s is the test statistic. \bar{Y} is the sample mean of the observed data, μ_o is the expected mean, and σ is the standard deviation observed data. The resulting test statistics could be used to determine the P-values and whether the DPIV system velocity and volume measurements are accurate.

Results

Volume Results

The volume of the expelled water is in the vortex ring (Kim & Gharib, 2011, T. Maxworthy, 1972). Both vortex ring cross section cores were visible in each area of interest; thus, D was measured as 0.009 ± 0.001 m. Once the six radii were measured from the core to the outermost boundary of the ring, they were averaged and used in the vortex ring volume equation; on average, the radii were 0.003 ± 0.001 m (Fig 2.4). The mean volume was compared with the expected volumes using the Pearson's chi-square test. The predicted volume was 1 mL and the observed volume was $98.8 \pm 1\%$ of the predicted. The two P-values were > 0.05 (Table 2.1), thus there was no significance between expected vs. measured volumes.

Velocity Results

The syringe pump produced flow at two velocities, and these velocities were estimated using the DPIV instrument and a polyline analysis beginning at 0.04 s after the initial water movement (Table 2.1). Analysis 0.04 s from the initial water movement ensured that the water was ejected and the ring vortex had formed. From the polyline analysis, the maximal velocities were recorded. For the ten trials, the velocities were averaged and compared with the syringe pump's test specifications (Eq. 4). The two predicted velocities were $0.016 \text{ m}\cdot\text{s}^{-1}$ and $0.026 \text{ m}\cdot\text{s}^{-1}$ and the observed velocities were $84.2 \pm 0.1\%$ and $96.2 \pm 0.1\%$, respectively. P-values were > 0.05 (Table 2.1), thus there was no significance between expected vs. measured velocities. The velocity was analyzed to show the accuracy and error of the DPIV measurements (Table 2.1).

Discussion

The DPIV system I describe here was economically designed to visualize water flow, especially vortex rings for biological and engineering applications. If one axis of a vortex ring is symmetrical, this planar DPIV system is good enough for measuring the core diameter and radius, if the light sheet is projected the axis of symmetry. The constraint on particle brightness was a key factor in determining which fluid flow velocities could be measured. With faster fluid flow, a combination of increased brightness, shorter laser pulses, or faster shutter speeds are required to prevent "streaking" of the illuminated particles in motion. Any lens with $< F = 1.4$ can be used on a high speed camera with the described laser power.

The parts for the DPIV system were not difficult to obtain, and most were reasonably priced. The household aquarium was a large enough to avoid boundary effects, as estimated by the velocity of water over a flat plate (Eq. 1). The aquarium tubing was inexpensive but flexible, and in concert with the compressible air in the syringes, constituted sources of error because of energy lost to those materials. The Pliolite particles were used due to their high reflectivity, animal compatibility, similarity to the density of water, and ease in altering the particle diameter. This DPIV system was economic because I adapted relatively high-powered laser-pointers as the illumination source. The economical benchtop power supply was more than enough to power the lasers. The higher-priced Phantom high-speed camera, which was priced at \$5000, was more than sufficient to perform DPIV due to its frame rate and digital image storage capacity. At its maximum aperture, the Nikkor lens was enough to capture the particle reflections. Alternative lenses at $\sim F = 1.4$ can be used, but the balance between laser brightness and lens aperture size should be considered. A new Kickstarter company

called “fps1000” has developed an economical digital camera with high-speed video capabilities and a frame rate up to $550 \text{ f}\cdot\text{s}^{-1}$ with a resolution of 1280×720 pixels, which can easily be modified for this DPIV system (Rowan, 2014). The DPIV software was adequate and user-friendly, however identifying vortex cores and boundaries proved challenging and was prone to user error. Repeating DPIV analyses on the same videos was important in limiting user error.

Ring’s economical DPIV instrument was developed to measure laminar fluid flow and determine where and why energy losses are occurring in dividing flow junctions for engineering education and applications. In their system, they suggest using a Casio high speed video camera Exilim Ex-ZR100 (Ring, B. P., et al. 2013). Resolution of Casio’s camera at 240 frames per second is 432×320 pixels. Although the Exilim Ex-ZR100 is cheaper, at around \$300, the fps1000 resolution for the price of \$1,500 may be better for research purposes.

A validation procedure was developed to test the DPIV system error using a vortex ring. The PIVlab software monitored the particle movement that represents the vortex ring. The software measures the core diameter, radius, and maximal velocity of the vortex ring (Fig 2.4). Using the Pearson’s chi-square test, the p-values showed no significant differences between expected volume and velocity results to measured ones.

DPIV systems have been developed to measure fluids related to biological systems. Economic DPIV systems for liquids have been mentioned (Ryerson & Schwenk, 2012); however, an economic system has not been previously assembled for use in biological systems.

This DPIV system described here can be applied to many types of investigations: various organisms that shed vortex rings in water, such as fish and frogs. Fish use their fins in rhythmic synchrony to shed linked vortex rings (Lauder et al., 2002, Shadwick & Lauder, 2006). Frogs, whether swimming with simultaneous or alternating kicks, shed a vortex ring from each foot (Stamhuis & Nauwelaerts, 2005). This DPIV system can be employed to estimate the volume (Eq. 3), velocity, mass ($m = \rho V$), acceleration ($a = \text{maximal velocity/time}$), force ($\text{force} = ma$), and kinetic energy ($\text{KE} = (0.5)mv^2$) of vortex rings shed from organisms that propel themselves under water. Although commercial DPIV systems may have fewer limitations, this system is accessible to more investigators worldwide due to its low cost and customizability.

References

- Flammang, B. E., Lauder, G. V., Troolin, D. R., and Strand, T. E. (2011). Volumetric imaging of fish locomotion. *Biology Letters* 7, 695–698.
- Kim, D., & Gharib, M. (2011a). Characteristics of vortex formation and thrust propulsion in drag-based paddling propulsion. *Journal of Experimental Biology*, 214, 2283-2291.
- Kim D., Gharib, M. (2011b). Flexibility effects on vortex formation of translating plates, *J. Fluid Mech.*, 677, 255–271.
- Lauder, G. V., Nauen, J. C., & Drucker, E. G. (2002). Experimental hydrodynamics and evolution: Function of Median Fins in Ray-Finned Fishes. *Integr. Comp. Biol.*, 42, 1009-1017.
- Maxworthy, T. (1972). The structure and stability of vortex rings. *Journal of Fluid Mechanics*, 51, 15-32.
- Nauwelaerts, S., Stamhuis, E., & Aerts, P. (2005). Swimming and leaping in a semi-aquatic frog. *Animal Biology*, 55(1), 3-15.
- Raffel, M., Willert, C. E., & Kompenhans, J. (2007). *Particle image velocimetry*. (2 ed.). New York, NY: Springer Publishing Company.
- Ring, B. (Director) (2013, July 1). Development of a Low Cost Particle Image Velocimetry System for Fluids . *ASME 2013 Fluids Engineering Division Summer Meeting*. Lecture conducted from American Society of Mechanical Engineers, Incline Village, NV.
- Rowan, G. (2014, October 1). fps1000 - The low cost high frame rate camera. Retrieved December 2, 2014, from <https://www.kickstarter.com/projects/1623255426/fps1000-the-low-cost-high-frame-rate-camera>
- Ryerson, W. G., & Schwenk, K. (2012). A simple, inexpensive system for digital particle image velocimetry (DPIV) in biomechanics. *Journal of Experimental Zoology*, 317, 127-140.
- Shadwick, R. E., & Lauder, G. V. (2006). *Fish biomechanics*. (Vol. 23, pp. 1-542). London, England: Elsevier Academic Press.
- Stamhuis, E. J., & Nauwelaerts, S. (2005). Propulsive force calculations in swimming frogs II. application of a vortex ring model to DPIV data. *The Journal of Experimental Biology*, 208, 1445-1451.
- Stamhuis, E. J., & Videler, J. J. (1995). Quantitative flow analysis around aquatic animals using laser sheet particle image velocimetry. *Journal of Experimental Biology*, 198, 283-294.
- Thielicke, W., and E. J. Stamhuis. 2012. PIVlab - Time-Resolved Digital Particle Image Velocimetry Tool for MATLAB. Ver. 1.32

Table 2.1: Velocity and volume measurements for vortex ring cross sections using digital particle image velocimetry. The experimental statistics and associated P-values were derived by comparing the observed means to the expected means using the Pearson's chi-square test.

Run	Velocity measurements at $0.016 \text{ m}\cdot\text{s}^{-1}$	Velocity measurements at $0.026 \text{ m}\cdot\text{s}^{-1}$	Volume measurements (1 mL) at $0.016 \text{ m}\cdot\text{s}^{-1}$	Volume measurements (1 mL) at $0.026 \text{ m}\cdot\text{s}^{-1}$
<i>One</i>	<i>0.016</i>	<i>0.027</i>	<i>0.978</i>	<i>1.029</i>
<i>Two</i>	<i>0.021</i>	<i>0.027</i>	<i>1.015</i>	<i>0.986</i>
<i>Three</i>	<i>0.023</i>	<i>0.021</i>	<i>1.021</i>	<i>0.996</i>
<i>Four</i>	<i>0.019</i>	<i>0.027</i>	<i>1.024</i>	<i>1.029</i>
<i>Five</i>	<i>0.017</i>	<i>0.025</i>	<i>0.999</i>	<i>1.040</i>
Average	0.019	0.025	1.007	1.016
s.e.m.	0.001	0.001	0.009	0.011
Expected velocity or volume	$0.016 \text{ m}\cdot\text{s}^{-1}$	$0.026 \text{ m}\cdot\text{s}^{-1}$	1.000 mL	1.000 mL
Exp. Statistic	2.550	-0.435	0.862	1.520
P-value	0.980	0.641	0.824	0.932

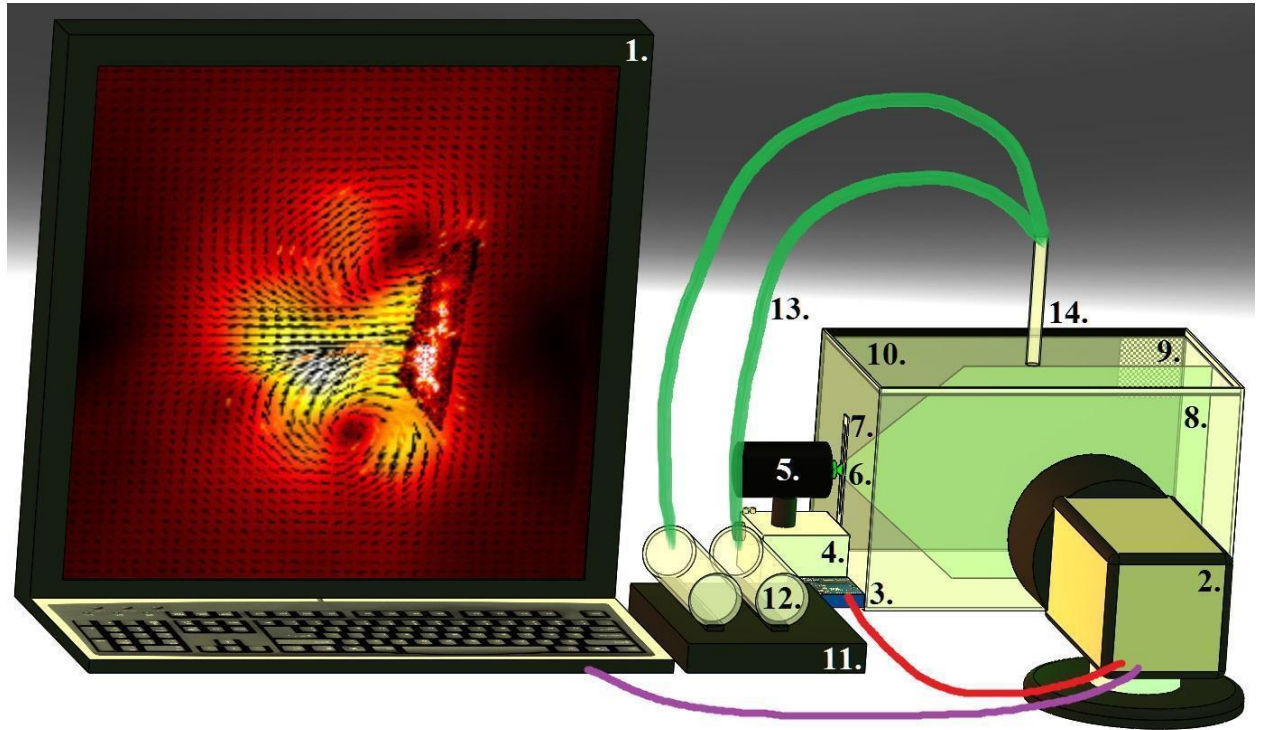
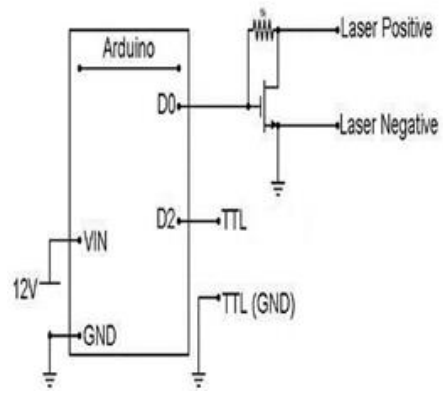
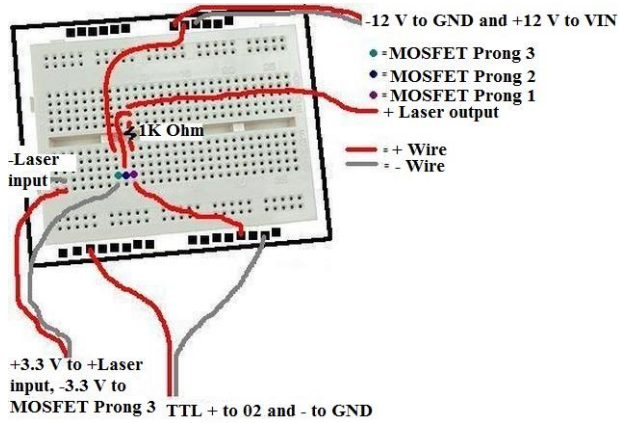


Figure 2.1: A simplified illustration of this DPIV instrument and the components necessary for Validation: 1. a desktop computer, 2. a high-speed camera, 3. a microprocessor, 4. a benchtop power supply, 5. a 0.8 W green laser pointer, 6. a cylindrical laser lens, 7. a vertical paper aperture, 8. the laser sheet, 9. grid paper, 10. an aquarium, 11. a dual-syringe pump, 12. a plastic syringe, 13. clear vinyl tubing, and 14. a glass vortex ejection cylinder.



(a)

(b)

Figure 2.2: Wiring (a) and circuit (b) schematics for the Arduino Uno used to synchronize the lasers and power source from the high-speed camera's TTL signal output (5 volts max.). (a) An illustrated example of the wiring in a breadboard, and (b) a circuit illustration. $12V$ indicates the 12 volts from the power supply. VIN is voltage in to the Arduino Uno. $D0$ is output to the lasers, and $D2$ is the TTL signal used to fire the lasers at the desired pulse rate.

```

// Laser Fire synchronizing program written by Kit Wilkinson and Russell Nelson

int pin = 13; // Indicates what initial pin was used.

volatile int preDelay = 10; // PreDelay, in  $\mu$ s, allows the camera shutter to open.

volatile int pulseWidth = 1250; // Pulsewidth in  $\mu$ s.

void setup() // Sets up the repeating sequence.
{
  pinMode(pin, OUTPUT); // Sets the pin to output mode.

  attachInterrupt(0, fireLaser, RISING); // Tells the Arduino the TTL signal is rising.
}

void loop()
{
  digitalWrite(pin, LOW); // Establishes the pulse is off during low TTL voltage (0-0.5 volts).
}

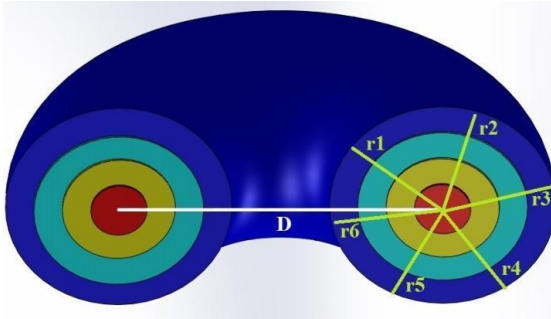
void fireLaser() // Synchronizes TTL signal to laser signal.
{
  delayMicroseconds(preDelay); // Sets the preDelay in  $\mu$ s.

  digitalWrite(pin, HIGH); // Establishes the pulse is on during high TTL voltage (2.7-5 volts).

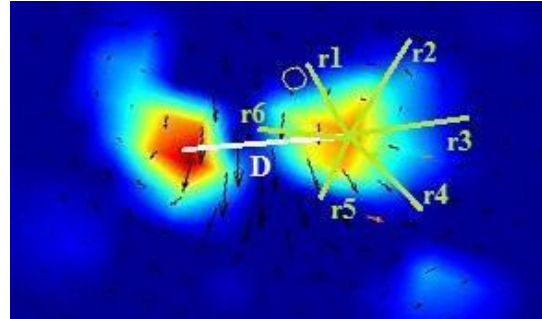
  delayMicroseconds(pulseWidth); Sets the pulseWidth in  $\mu$ s.
}

```

Figure 2.3. The program 'Laser Fire' code used to synchronize the laser pulse with the high-speed camera's TTL signal output using the Arduino Uno microprocessor.



(a)



(b)

Figure 2.4. A diagram (a) of a vortex ring with the core diameter (D) and 6 radii ($r1 - r6$) used to calculate the volume of the vortex rings. The radii were averaged to calculate the ring volume (Eq. 1). A real vortex ring (b) visualized using the DPIV software. The fastest velocity of rotation is represented by red, whereas blue the slowest velocity.

Chapter 3: Ballistic locomotion between media: A kinematic and kinetic analysis of a frog launching from water

Abstract

The locomotor transition from one medium to another is crucial to the survival of animals such as Orca and Kingfishers, which move through air and water, and on land. Anurans are animals that can move from land to water and vice versa due to their morphology and physiology. A handful of frogs leap from water into the air; this locomotion is not well-understood but is important for species with the ability to escape predators and capture prey. Bullfrogs been shown to leap from water into air to capture aerial prey or to escape water-filled depressions. Here, leaping on land and water are compared to describe how water leaping in bullfrogs is achieved. Biplanar, high-speed videography was used to record kinematics; these videos were used to measure joint extension duration, take-off velocity, and kinetic energy for land and water leaping. During a water leap, an elliptical vortex ring is shed from each from foot. The velocity and volume of these vortices were estimated using digital particle image velocimetry. The results show that the joints extended faster during the water leap; however, the joint extension sequence was the same. The take-off velocities and overall kinetic energies of both leaps did not significantly differ, which indicates that the leaping biomechanics in bullfrogs are capable for leaping in at least two different media.

Introduction

Many vertebrates, such as chameleons, ostriches and cheetahs have adaptations to move on land. This is also true for vertebrates that mainly move in water or air. Some species are able to cross over into different media. The benefits of moving through different media may include access to a greater variety or number of prey, eluding predators, and dispersal. Examples of animals that do so include orcas that strand to catch elephant seal pups on land and are able to move back into the water (Guinet & Bouvier, 1995), submerged Nile crocodiles that grapple shoreline gazelles as they drink from waterholes, and kingfishers that can dive into water from the air, catch a fish, breach the water's surface, and return to a perch (Whitfield & Blaber, 1978). Certain animals, such as the basilisk lizard can run across water; thus they are in two different media simultaneously (Glasheen & McMahon, 1996; Hsieh, 2003; Hsieh & Lauder, 2004). This ability is due to their structures and functions, which facilitates locomotion in different environments, however saltatorial locomotion at the air-water interface has largely been ignored.

Few vertebrates exceed frogs in their ability to move on land and in water. Nauwelaerts et. al. (2005 - 2007) found no direct evidence for trade-offs of hind-limb performance in leaping and swimming (Nauwelaerts et al. 2005, Nauwelaerts et al., 2007). Frogs can swim and leap due to the unusual design of their hindlimbs, which have been compared to a 'vertebrate catapult' (Astley & Roberts, 2012). The frog's catapult-like hindlimb facilitates stored elastic recoil energy from various parts of their skeletal-musculo-tendon system, which can be released simultaneously with muscle contraction during a leap. In addition, frog hindlimb muscle operating lengths are greater than in

other vertebrates (Azizi & Roberts, 2010), which facilitates greater storage of elastic recoil energy in tendons, fascicles, and intrinsic muscle proteins such as titin. The release of energy coupled with muscle contraction amplifies the power for ballistic locomotion (Peplowski & Marsh, 1997). Additionally, juvenile frogs tend to have muscle-tendon units with proportionately greater tendon weights than adults, which suggests that juvenile frogs may have higher power amplification than adults (James et. al., 2007).

Juvenile bullfrogs are capable of water and land leaps; these frogs can leap from the water to catch aerial insects and escape predators or water-filled depressions. During the water leap, the frog is nearly or entirely submerged.

The bullfrog is not the only anuran species that can leap from water. Goliath frogs (*Conraua goliath*) leap from water on the Nkebe river in central Africa (Herrmann, 2006). Nauwelaerts (2004) suggested the shape and curvature of the feet in Indian Skittering Frogs, *Euphlyctis cyanophlyctis* and *E. hexadactylus*, aid in their ability to water leap (Nauwelaerts et al. 2004).

The ability of frogs to move through different media not only requires musculo-tendon organs but also motor control plasticity from the central nervous system. Groups of neural unit burst generators, referred to as 'motor primitives' (Hart & Giszter, 2010) were observed in spinalized American bullfrogs, *Lithobates catesbeianus* (Shaw, 1802); these primitives control 80% of the frog's locomotor behaviors, including feeding lunges, leaping, and swimming. Evidence of the plasticity of these motor primitives is based on differing action potential timings that results in a variety of locomotor behaviors (Hart & Giszter, 2004).

Here, I investigate the biomechanics of anuran water leaping by comparing land leaping using kinematic and kinetic parameters. Kinematics were described with hindlimb joint extension sequences, start times, and durations. The kinetic energy was used to estimate the total work performed during both leaps; however, a few key differences in the water leap influences the total work and power that the hindlimbs must produce. These differences include but are not limited to drag, kinetic energy loss to the water through surface waves and vortex rings, and water moving with the frogs' bodies.

Materials and Methods

Animals

Wild, juvenile American bullfrogs, *Lithobates catesbeianus*, were tested in the field for their water leaping ability on September 28, 2012 at White Horse Lake, Arizona (Latitude: 35-07'01" N, Longitude: 112-00'49" W, at an elevation of 1,998 m). An aquarium (0.51 m x 0.25 m x 0.3 m) was filled with water to approximately two thirds of its volume. All frogs were weighed. 10 frogs were placed in the aquarium at a time to observe which ones would try to escape by leaping from the water. Of the 198 frogs tested, only 13 performed a water leap and were collected. Of the thirteen frogs, only three performed the water leap under laboratory conditions; thus, n=3.

The three frogs had 0.080 ± 0.005 m average snout-vent length (SVL) and 0.030 ± 0.005 kg body mass and were maintained in individual plastic terraria (0.31 m x 0.17 m x 0.09 m) with 0.01 m of water above 0.01 m of gravel in the Northern Arizona University (NAU) Small Animal Care facility. All frogs were fed a diet of crickets. The temperature in the holding and experimental rooms was 20°C with a 12 h light:12 h dark

photoperiod. The procedures were approved by NAU Institutional Animal Care and Use Committee (IACUC).

The Kinematics of Leaping on Land

High-speed videography was used to analyze the leaping frog kinematics (Marsh & John-Alder, 1994). The frogs were filmed using high-speed, black and white and color video cameras (Phantom V5.1 Vision Research, Inc., Wayne, NJ, USA) with lateral and dorsal perspectives, respectively. The cameras were synchronized and set to 250 frames·second⁻¹ (f·s⁻¹), and I used an exposure of 1/500 s, and an AFD Nikkor lens (Nikon Corp., Tokyo, Japan, $f = 0.05$ m, $F_{\min.} = 1.4$) using f /stop of 4 ($f/4$). Full spectrum light was provided by two 6 x 6 light-emitting diode arrays (LED) and two low-light, 9 x 9 LED camera-synchronized stroboscopic infrared arrays. A land-leaping platform (0.6 m x 0.33 m x 0.33 m) was constructed with an open front and top to gain access the frogs. A grid composed of 0.01 m squares was placed behind the leaping platform. Three clay bricks (0.2 m x 0.1 m x 0.06 m) were placed with the long sides touching as a substrate for the frogs to leap from. A fourth brick was stacked on top of the right-most brick to encourage the frogs to leap at an angle of at least 40°, and a horizontal length of at least 0.3 m. A 0.05 m x 0.05 m grid was placed on one of the bricks to calibrate the dorsal perspective. The frogs were lightly touched near their cloaca to induce a leap.

Three to four leaps per frog (a total of ten leaps) were included in the analysis. The videos that met the following criteria were included in the analysis: the frogs leaped perpendicular to the lateral camera perspective; propulsion was visible in both cameras from the starting position, in which the legs are closest to the body, through the full leg extension, including the metatarsals; the frogs cleared the stacked brick with a minimum

take-off angle of 40° to realize a horizontal distance; and both legs extended simultaneously. Each leap sequence was saved as a series of single-image files (Fig 3.4a) using the Phantom Camera Control Application (v2.41b Vision Research, Inc., Wayne, NJ, USA).

Kinematic analyses were performed using Didge 2.02 (A. Cullum, Creighton Univ., 2002) to manually monitor the anatomical points as a function of time, from which the amplitude and timing of the joint extension or flexion were digitized (Monroy & Nishikawa, 2000). Seven points on the frog were digitized for both the lateral and dorsal perspectives: the cloaca as well as the left and right longest toe tips, ankles, and knees. I obtained 3-D kinematics using the X and Y coordinates from the lateral perspective and the Y coordinate from the dorsal perspective. The X, Y, and Z coordinates were smoothed using a Butterworth filter at 40 Hz (Nauwelaerts et al. 2004).

Not all points were visible in each frame. Because the frogs leapt from left to right from the lateral camera's perspective, the frogs' left legs were not visible. Because the legs were extended simultaneously in the dorsal perspective, the digitized data from the right leg was used to represent both legs. In anurans, the cloacal velocity can be used as a proxy for the velocity of the center of mass (CoM) because the axial skeleton is more or less rigid (Marsh & John-Alder, 1994).

The Kinematics of Leaping in Water

The same frogs and cameras were used for kinematic analyses of water leaps. The only differences were that the maximum aperture of the lens was used, and the cameras were set to 125 f·s⁻¹ and an exposure of 1/250 s. A glass aquarium (0.41 m x 0.21 m x 0.25 m) was filled with water to a depth of 0.15 m (Fig 3.1). The ventral perspective of

the frogs was recorded using a mirror (0.3 m x 0.3 m) placed below the aquarium at a 45° angle. The ventral perspective was used instead of the dorsal perspective to avoid optical distortion effects caused by ripples on the water's surface. From the bottom of the aquarium to 0.03 m below the water's surface, the back of the aquarium was painted black for maximum contrast with the frogs' legs. Above the black paint level, a 0.01 m grid (0.2 m x 0.1 m) and a 0.005 m grid (0.05 m x 0.05 m) were placed in the bottom right hand corner of the aquarium to calibrate the distance. A resting platform was placed in the corner of the aquarium at a height of 0.14 m. A half-top cover was placed above the resting platform to entice the frogs to leap voluntarily from the water (Fig 3.1).

Only three to four leaps per frog (a total of ten leaps) were included in the analysis. The following criteria were used to select films for analysis: frogs leaped out of the tank from the water to a height of 0.1 m to ensure the frogs' bodies fully exited the water; the propulsion was visible from both camera perspectives, as defined for leaping from land; the take-off angle was $> 40^\circ$; the frogs leaped perpendicular to the lateral camera perspective; and the legs were simultaneously extended. The films were saved as a series of image files (Fig 3.4b). The kinematic analysis was the same as for the land leaps, except that the X, Y, and Z coordinates were smoothed using a Butterworth filter at 20 Hz.

The Kinetics of Leaping on Land

The collective musculo-tendon work provided the kinetic energy (KE) of the frog.

$$KE_{landfrog} = \frac{1}{2}mv_{to}^2 \quad (1)$$

$KE_{landfrog}$ (J) is the kinetic energy of the frog during the land leap. m is the mass (kg) of the frog, V_{to} is the take-off velocity of the frog ($m \cdot s^{-1}$). V_{to} is defined when the longest toes have left the brick.

The Kinetics of Leaping in Water

To obtain the kinetic energy of the frog in water ($KE_{waterfrog}$), the same method was used but with a few key differences. First, the friction of the frogs' bodies with the water is much greater than with the air. Second, the frogs were ~95-100% submerged before leaping. As the frog accelerates, the water closest to the frog's body also accelerates. The moving water is "added mass" and must be included in the mass term in the kinetic energy equation. Most of the added mass travels with the frog as it exits the water. In *Rana esculenta*, a frog with similar morphology to *L. catesbeianus* (Nauwelaerts et al., 2007), the added mass coefficient was 0.2; thus, I assumed here that the added mass coefficient is also 0.2. The $KE_{waterfrog}$ was calculated as follows.

$$KE_{waterfrog} = \frac{1}{2}(m + AMC(m))v_{to}^2 \quad (2)$$

$KE_{waterfrog}$ is the KE of the frog during the water leap, m is the mass of the frog, AMC is the added mass coefficient (0.2), and the V_{to} of the frog is in $m \cdot s^{-1}$. Further, drag acted on the frog bodies before they exited the water. Swimming *R. esculenta* exhibited a drag coefficient (C_d) of 0.14, which was determined using the deceleration rate in the glide phase during swimming (Nauwelaerts & Aerts, 2003). The key difference in C_d between a swimming frog and a water leaping one, assuming that the drag in the air is negligible due to the streamlined shape of the frog, is that the water leaping frog is exiting a more viscous medium.

An estimate of the required force to overcome drag was necessary to compare the work performed in both leaps because work equals force multiplied by distance a body travels. An estimate of the force required by the frog to overcome drag (F_d) is calculated as follows.

$$F_d = \frac{1}{2}(\rho)(v^2)(C_d)(A_c) \quad (3)$$

F_d is the force required to overcome water drag, ρ is the density of water, v is the velocity of the cloaca, C_d is the drag coefficient of a frog's body, and A_c is the mean cross sectional area of the frogs' bodies. To determine the work necessary to overcome drag (W_d), instantaneous power must be calculated because power is the rate of work. F_d was multiplied by the velocity of the cloaca for each frame during the propulsive phase. A power curve was drawn from each instantaneous power step (Fig 3.4d). The area under the power curve is the magnitude of work and was calculated, but because the frog was under water for roughly the first half of the propulsive phase, the area under the first half of the curve was added to each instantaneous kinetic energy step representing the added work the frog had to perform to overcome drag (Fig 3.4d).

The Vortex Kinetics

DPIV was used to calculate the mass and velocity of the vortex rings shed from a frog's foot, which I assumed included some but not most of the water KE (Johansson & Lauder, 2004; Stamhuis & Nauwelaerts, 2005). KE_{water} is the total kinetic energy imparted to the water, including compression, surface waves, and vortex rings. A custom DPIV system was used to investigate the mid-cross sections of the elliptical vortex rings to measure their shapes and estimate their masses and velocities. DPIV is an accepted method for quantifying the volume and velocity of the water flow phenomena used by

animals that propel themselves in water (Stamhuis & Videler, 1995). However, DPIV measurements underestimate kinetic energy of a vortex ring (KE_{vortex}) due to the energy loss from the foot and ring interface (Stamhuis & Nauwelaerts, 2005). To obtain the kinetic data from the water leap, a custom DPIV instrument was constructed. The purpose of the DPIV instrument was to measure the shape, volume and velocity of the vortex rings shed from the frogs' feet. Stamhuis & Nauwelaerts (2005) observed swimming *R. esculenta* and found that the vortex shed from a frog's foot is an ellipsoid ring. The rings' short and long axes exhibited a ratio of 1:1.75, the longer of which approximately matched the long axis of the foot. The vortex rings' short and long axes are perpendicular to the direction of the frog and translation of the vortex ring (Johannson & Lauder, 2004).

DPIV Methods

DPIV uses high-speed videography to record movements of illuminated, neutrally buoyant particles. A planar DPIV system was employed to measure the geometry and velocity of the ellipsoidal vortex rings.

DPIV software monitors the light reflected by illuminated particles from frame to frame (Thielicke & Stamhuis, 2012). The velocity of each particle can be calculated using the frames per second of the camera, and the calibration distance. Because the vectors within a vortex ring have a much higher velocity than the surrounding fluid, the software was used to create a 2-D cross section image (Fig 3.2a).

The aquarium used for DPIV was large enough to account for the boundary layer thickness < 0.001 m (Wilkinson, Ch. 2).

The water was seeded with approximately spherical, neutrally buoyant ($1030 \text{ kg}\cdot\text{m}^{-3}$), biologically compatible, reflective Pliolite (Eliokem, Inc., Akron, OH, USA) particles. The average Pliolite particle diameter was $6 \times 10^{-5} \text{ m}$, which was obtained through grinding in a blender and vibrating in a sieve tube. I used the concentration of $6 \times 10^{-6} \text{ g Pliolite}\cdot\text{H}_2\text{O m}^{-3}$, which provided adequate illumination to analyze the volume and velocity of the vortex rings with negligible effects on viscosity (Raffel et al., 2007). A 0.01 m grid on the back of the aquarium was used as a reference distance for digitization and DPIV (Fig 3.1).

A laser illumination system was constructed to visualize particle motions. Green laser light ($\lambda = 532 \text{ nm}$) originated from three high powered pen lasers (Wha Fat Technological Co., Ltd, Hong Kong, China, $P_{\text{max}} = 0.8 \text{ W}$). To construct a vertical light sheet, cylindrical lenses (Central Machinery, Shenzhen, China, $f = 0.004 \text{ m}$) were mounted on the lasers. Paper apertures (0.002 m wide) were placed vertically on the sides of the aquarium to absorb beams of light outside the sheet. The illuminated area of interest for DPIV analyses was 0.08 m x 0.08 m and was used to record the long-axis cross section of a vortex ring shed from a frog foot. The lasers were pulsed at ten times the frame rate of the camera to avoid interleaving effects. The lasers were synchronized using an Arduino Uno microprocessor (Smart Projects, Ivrea, Italy). The rising transistor-transistor logic signal from the high-speed camera was used for synchronization with custom code (Wilkinson, Ch. 2).

DPIV and kinematic data and were recorded simultaneously and saved as a series of images. The geometry, volume and velocity were analyzed using the same image series. The image series with the shed vortex ring was analyzed pairwise using PIVlab

1.3 (Thielicke & Stamhuis, 2011). Cross-correlation was performed using a convolution filter by applying a 90 x 45 pixel interrogation area for the first pass, a 70 x 35 area for the second pass, and a 50 x 25 area for the third. The convolution filter's pixel interrogation area was determined based on the density of particles relative to the cross-sectional area of the vortex ring. For finer resolution of the ring cross-section, two algorithms were used: contrast-limited adaptive histogram equalization to enhance image contrast and a high-pass filter that sharpened the image and removed background signals. Vectors over eight standard deviations from the mean were removed from the datasets. A cubic spline interpolation was used to smooth the datasets for DPIV data.

A planar arrangement of velocity vectors was used to calculate the volume and velocity of the vortex cross section; these parameters aid in describing and characterizing vortex ring phenomena (Stamhuis & Videler, 1995). To estimate the KE_{vortex} , the vortex was divided into a gridwise set of elements, each with a KE value ($KE_{vortexelement}$). To estimate the $KE_{vortexelement}$, the volume and velocity of each element was measured. To estimate the KE_{vortex} , the $KE_{vortexelement}$ were summed (Bartol et al., 2008) and multiplied by two because the frog has two feet.

To obtain the $KE_{vortexelement}$, the bottom side of the vortex ring cross section was divided into a grid of elements with vectors (Fig 3.2b). A rectangular prism with equal width and height was used to represent the distance between two equally spaced vectors. The ring's core diameter was measured as the distance between the two halves of the core (D). To obtain the length, the formula $2\pi(D/2)$ was used. However, an ellipsoid ring has two radii, one long and one short. To determine the average ring radius, the following formula was used.

$$r = 2\pi \sqrt{\frac{a^2 + b^2}{2}} \quad (4)$$

r is the average ring radius, a is the long radius, which measured using the DPIV instrument. I assume that the short radius (b) is 57% of the long radius (Stamhuis & Nauwelaerts, 2005). The volume was calculated using the radius estimates. I assumed that the rectangular prisms in the same row had the same estimated length from one side of the vortex to the other. However, the rectangular prisms closer to the middle of the vortex were shorter and composed the negative zone. The same concept was applied to rectangular prisms distal to the middle of the vortex and in the positive zone (Fig 3.2b).

For the mass of each rectangular prism, the density of water of $997 \text{ kg}\cdot\text{m}^{-3}$ was used. Once the mass was calculated, then the $KE_{vortexelement}$ could be determined. The KE_{vortex} was calculated using the following formula.

$$KE_{vortex} = 2 \left(\sum_{i=0}^n \left(KE_{vortexelement} = \frac{1}{2} mv^2 \right) \right) \quad (5)$$

KE_{vortex} is the total KE of both vortices, $KE_{vortexelement}$ is the KE of each element, m is the mass of each rectangular prism, and v is the magnitude of the velocity vector in a rectangular prism.

The Ex-vivo Foot

The DPIV analysis from the water leaps showed that the geometry of the vortices was not consistent. Before they leaped from the water, the frogs would swim, and swimming created flows that interfered with the vortices shed during leaping. Thus, it was impossible to calculate the vortex volume during leaping using our DPIV system.

To overcome this problem, a robotic frog foot was used to simulate the vortex rings produced by a frog foot during a leap from water. The robotic foot shed an ellipsoidal vortex ring.

As paddling propulsors, the feet create non-linked vortex rings. Development of the vortex ring depends on two distinct types of flow: spanwise and tip vortex. Spanwise flow includes the trailing and leading flow of water behind and in front of the foot, respectively. The tip vortex includes rotational flow of water around the edges of the foot in a horseshoe shape. The tip vortex depends on the characteristics of the spanwise flow. Spanwise flow depends on the propulsor velocity and shape (Kim & Gharib, 2011). Thus, I assume that the vortex ring shed from the frog foot depends on the velocity of the foot as it moves through water and on the foot shape (Aerts & Nauwelaerts, 2009).

I used real feet to accurately simulate the frog foot shape. The three frogs that leaped from the water in the laboratory were euthanized in a solution of 1.5⁻⁴% tricaine methanesulfonate (MS-222) for 30 min. and double-pithed. The left foot was then excised at the ankle joint. The feet were placed onto a rubber block and pinned with the webbing expanded as much as possible without damaging the foot. I was careful to maintain their natural curvature. The feet were preserved in 10% formaldehyde. Five days later, the feet were fixed in a splayed position, and the tibiae as well as the fibulae were removed using a drill press and dremel tool. A perforated steel rod with a diameter at approximately half the midfoot diameter was inserted in the hole. Silk suture was used to attach the foot to the steel rods. The length was adjusted such that the distance from the longest toe tip to the edge of the steel rod was 0.17 m for each foot. The steel rod was then attached to a servomotor.

A high-precision servomotor (HK Mi Series, HobbyKing.com, Lakewood, WA, USA) was used to move the *ex vivo* foot in the DPIV instrument and was controlled by the Arduino Uno microcontroller. The foot velocity was programmed to match the average velocity of the frogs' longest toes ($2.325 \pm 0.087 \text{ m}\cdot\text{s}^{-1}$ estimated at the longest toe tip) during propulsion. The resolution of the microcontroller and servomotor were not fine enough to realize $2.325 \text{ m}\cdot\text{s}^{-1}$ but moved the feet at $2.825 \pm 0.246 \text{ m}\cdot\text{s}^{-1}$ ($P = 0.040$), which I calculated based on kinematic analyses of the preserved feet as they were moved through the water.

A statistical analysis revealed that the live frog's toes mostly move in an arc; this analysis was performed by fitting the best plane, which was based on the principal component, to a set of points in a Cartesian coordinate system. The points were first centered by subtracting the mean vector (\bar{X} , \bar{Y} , and \bar{Z}). Second, an R^2 value was calculated as the proportion of variation about the mean of the points in 3-D, which is explained by the 2-D fit. The average R^2 was 99.67%; thus, the medial-lateral plane included only slight movement. Although the *ex vivo* foot arc radius was larger than the live frog foot arc during the water leap, they both exhibited the same propulsor shapes and similar velocities.

The servomotor and the attached *ex vivo* feet were used to produce vortex rings. The system was constructed such that the foot arcs were parallel to the vertical laser sheet in the DPIV system, dividing the foot into right and left regions. DPIV analyses were used to visualize the long axis of the ellipsoidal vortex ring. Five experiments for each *ex vivo* foot were filmed (fifteen total films). The DPIV analysis was the same as for the *in vivo* leaps from water. Although the arcs of the living and preserved toes were different, I

believe that the KE_{vortex} can be estimated using the *ex vivo* data due to the similar toe velocity and propulsor shape.

Results

Morphometrics

The average mass of the three leaping frogs was 0.032 ± 0.001 kg, and the SVL was 0.076 ± 0.001 m. Notably, for the field experiments, in the 198 frog population, no frog over 0.11 kg was observed to water leap. Thus, the frogs were small compared with adult *L. catesbeianus*, which can exceed 0.5 kg and 0.15 m.

The Land Leap Kinematics

The propulsion duration was defined as the moment the CoM began to move until the longest toes left the ground. The overall mean propulsion duration was 0.079 ± 0.011 s (Table 3.1).

The first joint to begin extending was the hip, which denoted the start of propulsion. The hip and propulsion duration were equal because the complete extension of the hip coincided with the legs straightening ($L_{straighten}$). The knee began extending after the hip by 0.047 ± 0.007 s, on average, and the extension duration was 0.034 ± 0.004 s. The mean ankle start time was 0.050 ± 0.009 s, which was followed closely by the knee, and the mean duration of the ankle was 0.030 ± 0.003 s. The longest toe tip remained stationary and was the last point to leave the ground. At a certain point, the three joints studied extended simultaneously and continued to extend together until $L_{straighten}$ (Fig 3.4c), which was also observed in *Rana esculenta* (Nauwelaerts et al. 2005).

The frogs' mean take-off velocity (V_{to}) was 3.416 ± 0.427 m·s⁻¹ during the land leap, which was calculated using the cloaca to estimate the velocity of the CoM (Table

3.1). V_{to} was the performance measure used to compare the leaps and was calculated using the frame immediately following the $L_{straighten}$. V_{to} was also used to calculate the $KE_{landfrog}$. These leaps were not maximal; the V_{to} remained fairly constant between the frogs and leaps. The velocity was highest in the frame following $L_{straighten}$, and I assumed that the frog had the available kinetic energy from the leap.

The Water Leap Kinematics

A key difference between land and water leaps is that the water leap included a preparative movement. The sequential pre-phase movements that were measured included the following: 1. the complete flexion of the hip, knee, and ankle joints. 2. The elbow fully extended with the shoulder when the arms were rotated inferiorly. 3. Because the pre-phase movements occurred at least four seconds before propulsion, I assumed that all momentum had dissipated and did not affect propulsion (Fig 3.3).

The hip extension indicated beginning of propulsion and the durations of these coincided. The knee began extending after the hip by 0.026 ± 0.003 s, on average, and the extension duration was 0.022 ± 0.003 s. The mean ankle start time was 0.027 ± 0.002 s, which was followed closely by the knee, and the mean duration of the ankle was 0.021 ± 0.002 s (Fig 3.4c). A major difference between the two leaping modes was that the longest toe tip began to make its arc for the duration of propulsion at an average max. velocity of 2.325 ± 0.087 $m \cdot s^{-1}$; whereas for the land leap the longest toe tips remained stationary until toe-off. At the end of propulsion, the foot collapsed its webbing by touching digits one and five. At a certain point, the three joints studied extended simultaneously and continued to extend simultaneously until the $L_{straighten}$. The overall mean propulsion duration was 0.048 ± 0.003 s (Fig 3.4c).

The mean V_{to} of the frog during the water leap was calculated using the cloacal velocity and was $3.179 \pm 0.546 \text{ m}\cdot\text{s}^{-1}$. The V_{to} was also used to calculate the $KE_{waterfrog}$. The velocity was highest in the frame following $L_{straighten}$, and I assumed that the frog had the available KE from the leap. The land and water leaps V_{to} were compared using a t-test, which showed no significant difference (Table 3.1).

The Land Leap Kinetics

KE was used to represent the total work performed by the hindlimbs' skeletal muscle-tendon units in a ballistic movement minus gravitational acceleration, and neglecting the air drag. The $KE_{landfrog}$ was determined based on the mean frog mass and mean V_{to} . The average $KE_{landfrog}$ was $0.188 \pm 0.030 \text{ J}$.

The Water Leap Kinetics

For $KE_{waterfrog}$, the frog hindlimbs were powerful enough to overcome the drag and move the body out of the water. The average $KE_{waterfrog}$ was $0.213 \pm 0.033 \text{ J}$. The $KE_{landfrog}$ and $KE_{waterfrog}$ did not differ when compared using a t-test (Table 3.1).

The Vortex Kinetics

Ellipsoidal vortices were filmed using the *ex vivo* foot and DPIV system. To stop the foot, the servomotor required a mean $0.032 \pm 0.003 \text{ s}$; the spanwise flow and tip vortices were combined to produce an elliptical vortex ring. The long axis of the vortex was clearly visualized using the DPIV software (Fig 3.2a). The long diameter of the vortex ring was measured, and its radius was used to determine the $KE_{vortexelement}$ zones for the rectangular prisms. The diameter was measured on the horizontal plane, which included zone zero (Fig 3.2b). Because the width and height of each element were the same ($5.340 \times 10^{-3} \text{ m}$), I was only required to determine the length. I determined the

average radius using equation 3, and the rectangular prism lengths were calculated using the formula $2\pi R$. In zone zero, the mean radiuses were enough to calculate the length of rectangular prisms in that row and were 0.081 ± 0.005 m. However, in negative zone one, I adjusted the radius because the row of rectangular prisms closer to the vortex' center had a shorter length by one rectangular prism width (5.340×10^{-3} m) thus, less volume.

Because the length, width, and height of each $KE_{vortexelement}$ were known, the volume was calculated. The mass of water in each rectangular prism was calculated using the density of water at 25°C ($997 \text{ kg}\cdot\text{m}^{-3}$) multiplied by the volume. The center of each rectangular prism width and height included a vector value calculated using PIVlab software in $\text{m}\cdot\text{s}^{-1}$. Because the velocity and mass were known, the kinetic energy of each element was calculated, summed, and multiplied by two (Eq. 5). The mean KE_{vortex} was 0.0142 ± 0.0037 J. The mean kinetic energy in the water imparted to the vortex rings was only 7.3 percent compared with the mean $KE_{waterfrog}$.

Overcoming drag in the water required extra energy for the first half of the propulsive phase. To estimate the work required to overcome drag, the instantaneous force to overcome drag (F_d) was calculated for each frame. Multiplying F_d by the cloacal velocity gave power for each step (P_d). The first half of the area under the P_d curve was calculated as 0.017 J, and this value was added to the KE values at each time step, which yielded the work required to overcome the drag (Fig 3.4d).

Discussion

Many vertebrates can transition between land and water and vice versa to exploit prey and avoid predators. Some vertebrates can move between water and air using wings or fins (Guinet & Bouvier, 1995, Whitfield & Blaber, 1978).

Frogs leap on land and generate propulsion during swimming by using their hindlimbs. Having large feet surface areas with catapult-like hindlimbs used for leaping allows for paddle-based propulsion (Jackson, 1992) in water with ballistic potential. Most of anuran locomotion is controlled from a relatively small portion of neurons in the brainstem (Hart & Giszter, 2010). Relatively simple signals from this region contribute greatly in many behaviors such as swimming and leaping (Hart & Giszter, 2004), suggesting that the plasticity of this control could be used for other locomotor purposes.

Before a frog jumps on land, it flexes the joints in the hindlimbs, thus stretching out extensor muscles and their tendons, storing elastic recoil energy (Astley & Roberts, 2012). Once the hindlimbs' extensor muscles begin to contract the stored elastic energy is released simultaneously. In addition, anuran muscles have been considered to have some of the fastest contraction velocities (Marsh, 1994). The hips begin to extend first, followed by the knee and then the ankle (Nauwelaerts et al., 2005). Once the legs are straight and the longest toe tips have left the ground, no more work can be performed on the solid ground. The V_{t0} was comparable to other studies of bullfrogs of similar mass, which suggests the amount of work performed by the hindlimb muscles was not usually more (Marsh, 1994). This results in a powerful leap and is important locomotion for the frog to avoid predators, catch prey, find a mate, and thermoregulate.

Leaping from water is different than leaping from land. Water moves when a force is applied. Anuran feet have relatively large surface areas compared to other tetrapods but will slip back if the force is applied to water. Water leaping is fundamentally different than how basilisks run on water because their bodies are above the water and their feet enter the water from the air (Glasheen & McMahon, 1996; Hsieh,

2003; Hsieh & Lauder, 2004). Drag is a factor when calculating total work because water leaping frogs have to overcome it. Another factor is an added mass of water surrounding the body that the frog must accelerate in addition to body mass. Because of the feet slipping backwards, drag and the added mass, the V_{to} should be less than leaping on land or the frog must produce more power to leave the water. *Euphlyctis cyanophlyctis* and *E. hexadactylus* are two species of frogs known to water leap. It has been shown that these species have shorter feet lengths when compared to *R. esculenta*, but other normalized morphometrics did not differ. Water leaping *Euphlyctis* hindlimb joint extension sequence was the same as *L. catesbeianus*. *Euphlyctis* was observed to have a V_{to} of $2.9 \text{ m}\cdot\text{s}^{-1}$ (Nauwelaerts et al., 2005) which was similar to *L. catesbeianus* V_{to} of $3.2 \text{ m}\cdot\text{s}^{-1}$.

Land leaping bullfrog acceleration and power outputs compared to other species of frogs and burst running lizards are comparable. Bullfrogs can attain an acceleration, which is mean V_{to} divided by the mean duration of the leap, of $43.24 \text{ m}\cdot\text{s}^{-2}$. An estimate of force could then be calculated as the mean mass of the frogs multiplied by mean acceleration. Using the ballistics formula for distance equals V_{to}^2 divided by gravitational acceleration. Once the distance was known, multiplying force by distance yielded work. Power is calculated as the rate of work and was $147.8 \text{ W}\cdot\text{kg}^{-1}$ at a 45° take-off angle. Adult *Limnodynastes peronii*, smaller frogs $\sim 0.02 \text{ kg}$ compared to the bullfrogs I studied, were calculated to have mean acceleration of $53.3 \text{ m}\cdot\text{s}^{-2}$ and mean power output of $\sim 200 \text{ W}\cdot\text{kg}^{-1}$ at a 45° take-off angle (Wilson et al. 2000). A lizard with similar mass, *Dipsosaurus dorsalis*, at $0.026 \pm 0.056 \text{ kg}$ produced $153.7 \text{ W}\cdot\text{kg}^{-1}$ in a single stride at 40°C , which is the lizard's preferred temperature (Swoap et al. 1993). Although

morphometrics in anurans is highly conserved, the elastic recoil energy storage mechanisms seen in anurans may exist in other animals to produce ballistic locomotion.

The propulsion joint extension sequence did not differ in either leaping mode. In swimming *R. esculenta*, the hip, knee, and ankle start to extend simultaneously during propulsion (Nauwelaerts et al. 2005), which suggests water leaping is less like swimming.

The difference in V_{to} for both leaps was not significant. The frogs that leapt in water were heavier due to added mass and were required to address gravity and drag. However, due to the large paddle surface area of the feet, this velocity was realized. A slower velocity may not allow the frog to generate enough kinetic energy to overcome drag or break surface tension. If the V_{to} and overall work from the hindlimbs is not different between the two leaping modes, but water is moved, then the power output for the hindlimbs must be higher in water leaping and may be close to the maximal. The hindlimb joint propulsion duration for the water leap totaled ~60% of the land leap duration, which indicates that the average power output for the muscle-tendon-bone units was nearly twice as high.

The difference in the frogs' propulsive kinetic energy at $L_{straighten}$ in both leaps was not significant ($P = 0.638$). During the water leap, enough kinetic energy is obtained to leap a similar distance as during a land leap, if the take-off angle is the same. If this amount of kinetic energy is required to escape predators and capture prey on land, then it stands to reason that the same will be true for the water leap.

The transfer of KE during propulsion from the feet to the two elliptical vortex rings was only 7.3 percent. These data indicate that, hydrodynamically, this system is

much more complex than previously thought, however does agree that DPIV is bound to underestimate the amount of energy imparted to water from a moving solid (Stamhuis & Nauwelaerts, 2005). To understand how the feet and body move the water, other types of DPIV instruments may be useful for future investigations.

Analyzing the biomechanics of water leaping may help further understand how animals use transitioning from one medium to another to survive and reproduce.

References

- Astley, H. C., & Roberts, T. J. (2012). Evidence for a vertebrate catapult: elastic energy storage in the Plantaris tendon during frog leaping. *Biology Letters*, *8*(3), 386-389.
- Azizi, E., & Roberts, T. J. (2010). Muscle performance during frog leaping: influence of elasticity on muscle operating lengths. *Proceedings of the Royal Society*, *277*, 1523-1530.
- Bartol, I. K., Krueger, P. S., Thompson, J. T., & Stewart, W. J. (2008). Swimming dynamics and propulsive efficiency of squids throughout ontogeny. *Integrative and Comparative Biology*, *48*(6), 720-733.
- Glasheen, J. W., & McMahon, T. A. (1996). A hydrodynamic model of locomotion in the basilisk lizard. *Letters to Nature*, *380*, 340-342.
- Guinet, C., & Bouvier, J. (1995). Development of intentional stranding hunting techniques in killer whale (*Orcinus orca*) calves at Crozet Archipelago. *Canadian Journal of Zoology*, *73*(1), 27-33.
- Hart, C. B., & Giszter, S. F. (2004). Modular premotor drives and unit bursts as primitives for frog motor behaviors. *The Journal of Neuroscience*, *24*(22), 5269-5282.
- Hart, C. B., & Giszter, S. F. (2010). A neural basis for motor primitives in the spinal cord. *The Journal of Neuroscience*, *30*(4), 1322-1336.
- Herrmann, H. W. (2006). *Conraua goliath* (Goliath Frog) leaping in water locomotion. *Herpetological Review*, *37*(2), 2006.
- Hsieh, T. S. (2003). Three-dimensional hindlimb kinematics of water running in the plumed basilisk lizard (*Basiliscus plumifrons*). *The Journal of Experimental Biology*, *206*, 4363-4377.
- Hsieh, T. S., & Lauder, G. V. (2004). Running on water: Three-dimensional force generation by basilisk lizards. *Proceedings of the National Academy of Sciences*, *101*(48), 16784-16788.
- Jackson, P. (Director) (1992, December 11). The Hydrodynamics of Paddle Propulsion. *11th Australasian Fluid Mechanics Conference*. Lecture conducted from University of Tasmania, Hobart, Australia.
- James, R. S., Navas, C. A., & Herrel, A. (2007). How important are skeletal muscle mechanics in setting limits on leaping performance? *Journal of Experimental Biology*, *210*, 923-933.
- Johansson, C. L., & Lauder, G. V. (2004). Hydrodynamics of surface swimming in leopard frogs (*Rana pipiens*). *Journal of Experimental Biology*, *207*, 3945-3958.
- Kim, D., & Gharib, M. (2011). Characteristics of vortex formation and thrust propulsion in drag-based paddling propulsion. *Journal of Experimental Biology*, *214*, 2283-2291.
- Marsh, R. (1994). Jumping Ability of Anuran Amphibians. *Advances in Veterinary Science and Comparative Medicine*, *B 38*, 51-111.
- Marsh, R. L., & John-Alder, H. B. (1994). Leaping performance of hylid forms measures with high-speed cine film. *Journal of Experimental Biology*, *188*, 131-141.

- Monroy, J. A., & Nishikawa, K. C. (2000). Aiming during prey capture in Microhylid frogs. *American Zoologist*, 40:6A.
- Nauwelaerts, S., & Aerts, P. (2003). Propulsive impulse as a covarying performance measure in the comparison of the kinematics of swimming and leaping in frogs. *Journal of Experimental Biology*, 206, 4341-4351.
- Nauwelaerts, S., Scholliers, J., & Aerts, P. (2004). A functional analysis of how frogs leap out of water. *Biological Journal of the Linnean Society*, 83, 413-420.
- Nauwelaerts, S., Ramsay, J., & Aerts, P. (2007). Morphological correlates of aquatic and terrestrial locomotion in a semi-aquatic frog, *Rana esculenta*: no evidence for a design conflict. *Journal of Anatomy*, 210, 304-317.
- Nauwelaerts, S., Stamhuis, E., & Aerts, P. (2005). Swimming and leaping in a semi-aquatic frog. *Animal Biology*, 55(1), 3-15.
- Peplowski, M. M., & Marsh, R. L. (1997). Work and power output in the hindlimb muscles of Cuban tree frogs *Osteopilus septentrionalis*. *Journal of Experimental Biology*, 200, 2861-2870.
- Stamhuis, E., & Nauwelaerts, S. (2005). Propulsive force calculations in swimming frogs II. Application of a vortex ring model to DPIV data. *The Journal of Experimental Biology*, 208, 1445-1451.
- Stamhuis, E. J., & Videler, J. J. (1995). Quantitative flow analysis around aquatic animals using laser sheet particle image velocimetry. *Journal of Experimental Biology*, 198, 283-294.
- Swoap, S. J., Johnson, T. P., Josephson, R. K., & Bennett, A. F. (1993). Temperature, muscle power output and limitations on burst locomotor performance of the lizard *Dipsosaurus dorsalis*. *The Journal of Experimental Biology*, 174(1), 185-197.
- Thielicke, W., and E. J. Stamhuis. 2012. PIVlab - Time-Resolved Digital Particle Image Velocimetry Tool for MATLAB. Ver. 1.32
- Whitfield A.K. and Blaber S.J.M., 1978. Feeding ecology of piscivorous birds at Lake St Lucia, part 1: diving birds. *Ostrich*, 49, 185-198.
- Wilson, R. S., Franklin, C. E., & James, R. S. (2000). Allometric scaling relationships of jumping performance in the striped marsh frog *Limnodynastes peronii*. *Journal of Experimental Biology*, 203(12), 1937-1946.

Table 3.1. A comparison of the land and water leaps in terms of the joint extension start times from the start of the propulsion, the joint extensions and propulsion durations, the take-off velocity (V_{to}), the maximum toe tip velocity, and the total kinetic energy. The P-values were derived from a pairwise, two-tailed t-test, which was used to compare the land and water leaps.

	Land Leap	Water Leap	P-value
Videos			
<i>Frog one</i>	4	3	
<i>Frog two</i>	3	3	
<i>Frog three</i>	3	4	
Propulsive Phase			
Joint extension start times			
<i>Hip (s)</i>	0	0	
<i>Knee (s)</i>	0.047 ± 0.007	0.026 ± 0.003	0.025
<i>Ankle (s)</i>	0.050 ± 0.009	0.027 ± 0.002	0.030
Durations			
<i>Hip (s)</i>	0.079 ± 0.011	0.048 ± 0.003	0.021
<i>Knee (s)</i>	0.034 ± 0.004	0.022 ± 0.003	0.036
<i>Ankle (s)</i>	0.030 ± 0.003	0.021 ± 0.002	0.025
<i>P-phase (s)</i>	0.079 ± 0.011	0.048 ± 0.003	0.021
Velocities			
$V_{to} (m \cdot s^{-1})$	3.416 ± 0.427	3.179 ± 0.546	0.737
<i>Max. toe tip (m·s⁻¹)</i>	0	2.325 ± 0.087	0.001
Kinetics			
<i>Kinetic energy of frog (J)</i>	0.188 ± 0.03	0.212 ± 0.033	0.638
<i>Kinetic energy of media (J)</i>	~0	0.014 ± 0.004	0.002

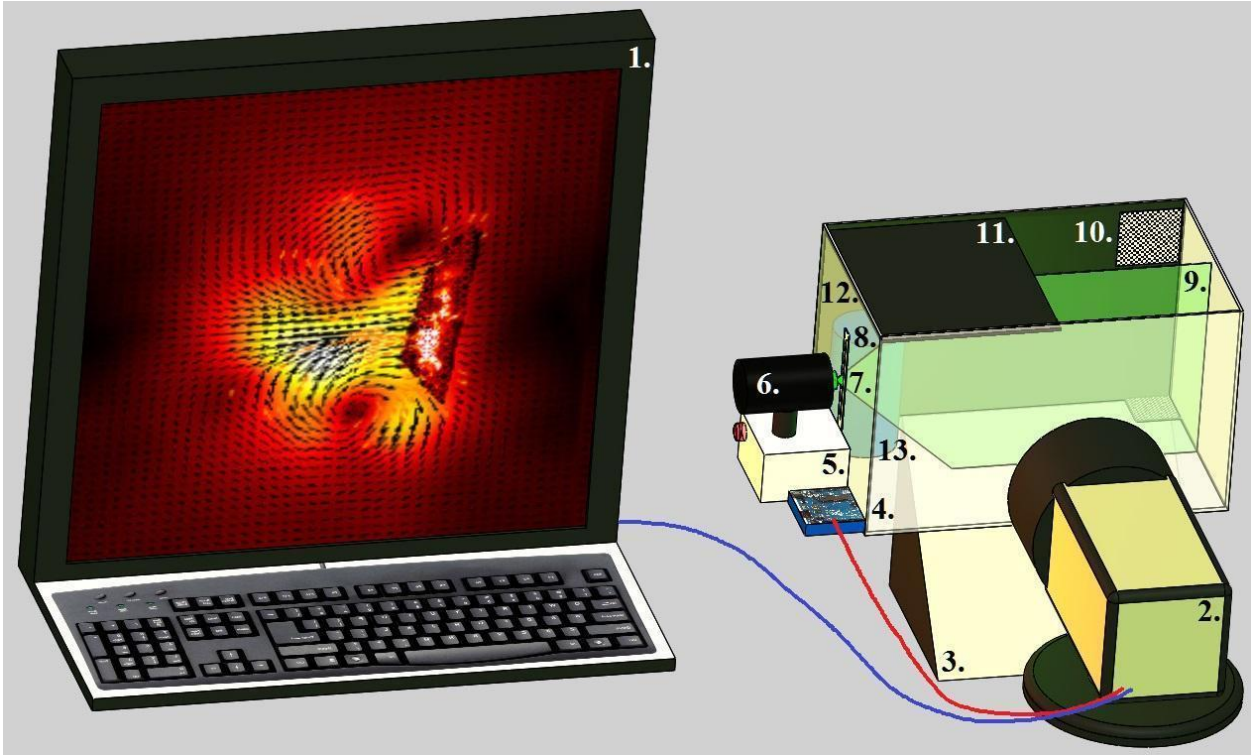
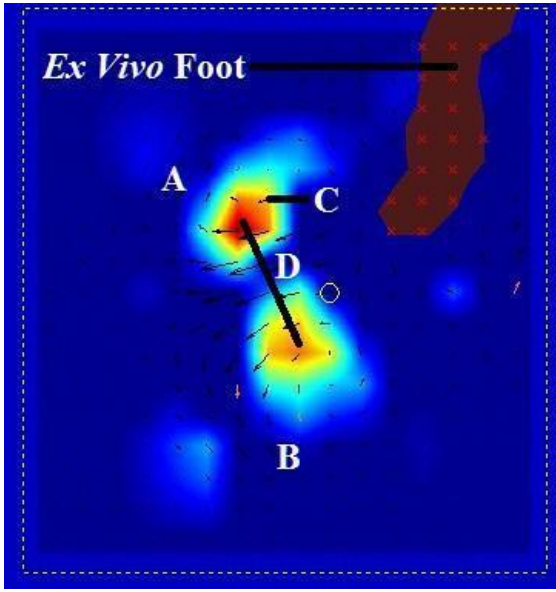
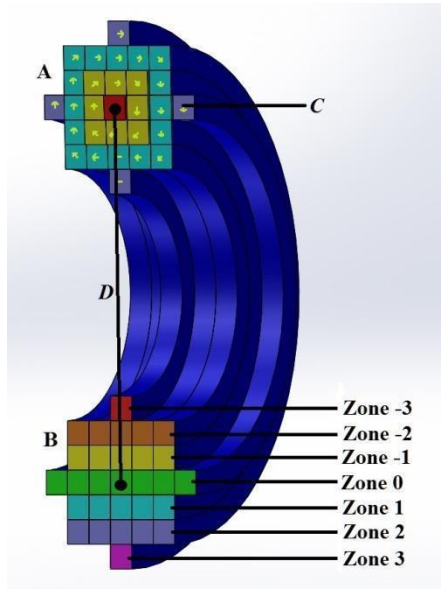


Figure 3.1: An illustration of the DPIV instrument: 1. a desktop computer, 2. a high-speed camera, 3. a 0.3 m x 0.3 m mirror placed at 45°, 4. a microprocessor used to synchronize the camera to the laser pulse, 5. a power supply, 6. a 0.8 W, 532 nm pen laser, 7. a cylindrical laser lens, 8. a paper aperture, 9. the laser sheet, 10. grid paper, 11. a plastic half-top cover, 12. a glass aquarium, and 13. a resting platform.



(a)



(b)

Figure 3.2. Cross section of a vortex ring shed from an *ex-vivo* foot in PIVlab 1.3 (a). Each arrow is a velocity vector; longer arrows indicate a higher magnitude velocity vector. The yellow arrows are interpolated vectors. The yellow circle highlights a single vector for analysis. A 3-D rendering of the cross section was then used to visualize the vortex ring (b). A vortex core row (Zone 0) was established on the bottom half of the vortex ring. From this row, negative and positive zones were identified. Once the zones were identified, the mass of each rectangular prism was determined. The kinetic energy was calculated using the vector in the center of the rectangular prism. The rectangular prism kinetic energy values were then summed and multiplied by two, which yielded the total kinetic energy for a vortex ring from a frog during a leap from water. (A) is the top half of the vortex, (B) is the bottom half, (C) is the vector arrow, and (D) is the core diameter

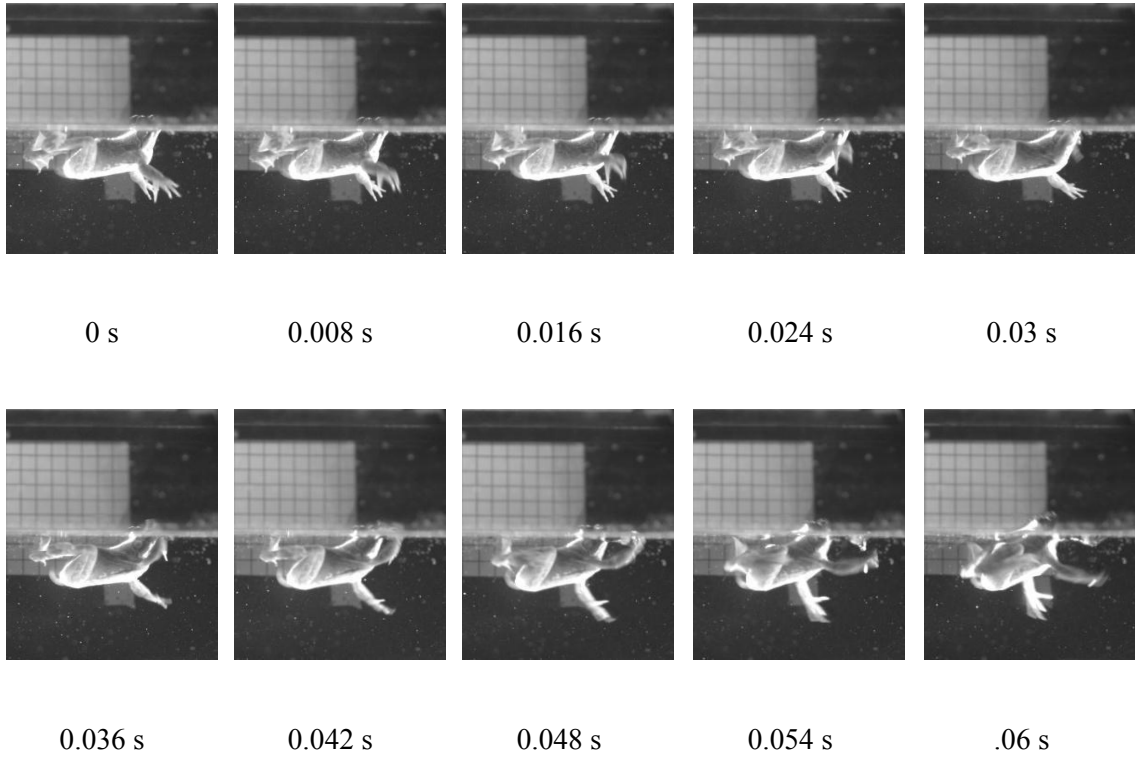


Figure 3.3. A series of images for the preparative phase of the water leap. The time is shown below the image. In the image series, the water level is shown as a horizontal line approximately midway from the top and bottom.

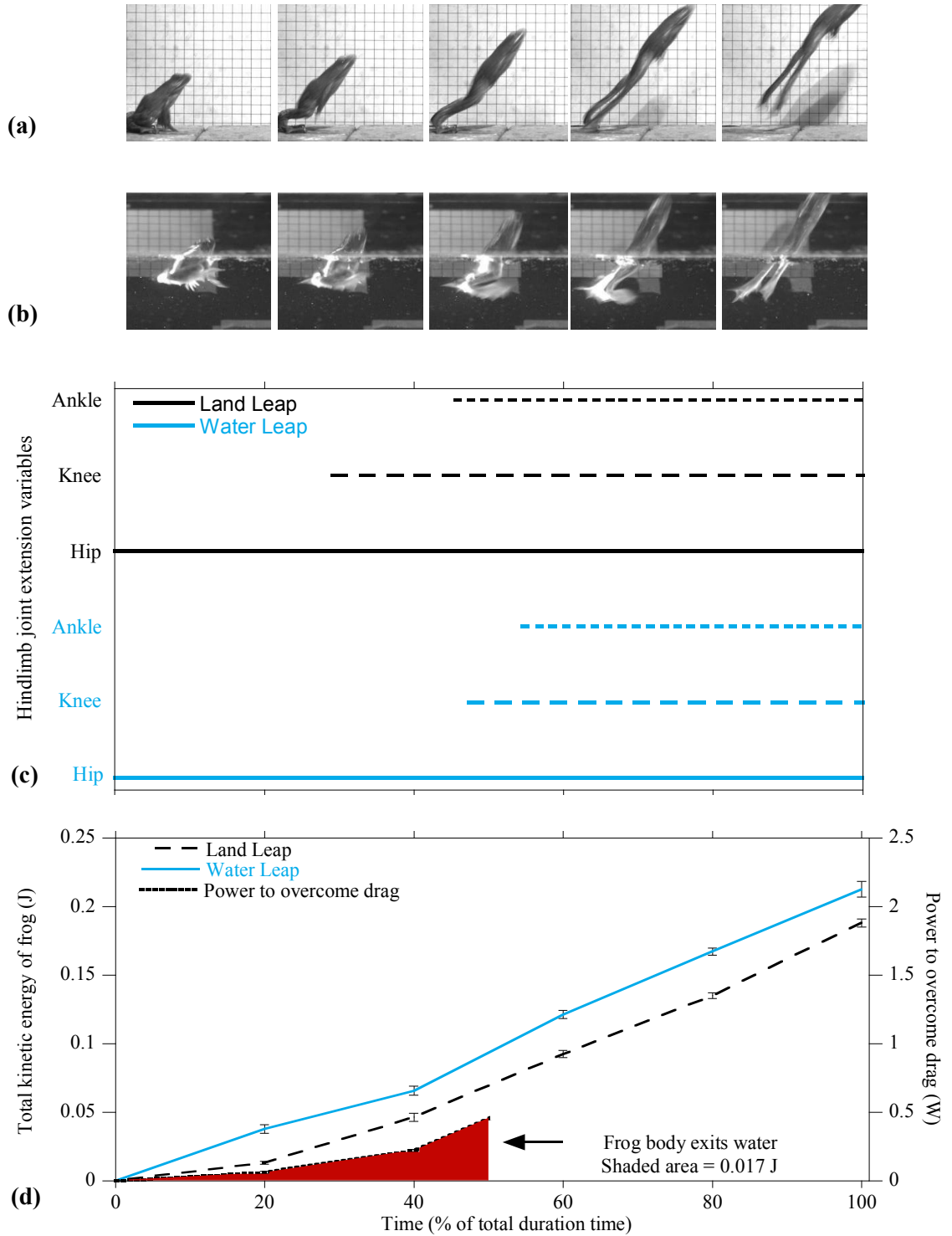


Figure 3.4. Frog hindlimb joint extension start, stop, and durations (c) and kinetic energy profiles (d) with a pictorial comparison of land (a) and water (b) leaps in % of propulsion time.

Chapter 4: Conclusions

Many vertebrates transition between land and water and vice versa to exploit prey and avoid predators. Some vertebrates can move between water and air using wings and fins (Guinet & Bouvier, 1995, Whitfield & Blaber, 1978).

Frogs generate propulsion by using their hindlimbs. Having large feet surface areas with catapult-like hindlimbs used for leaping allows for paddle-based propulsion (Jackson, 1992) in water with ballistic potential. Most of anuran locomotion is controlled from a relatively small portion of neurons in the brainstem (Hart & Giszter, 2010). Relatively simple signals from this region contribute greatly in many behaviors (Hart & Giszter, 2004), suggesting that the plasticity of this control could be used for other purposes.

Before a frog jumps on land, it flexes the joints in the hindlimbs, storing elastic recoil energy in their musculo-tendon-bone units (Astley & Roberts, 2012). Once the hindlimbs' extensor muscles begin to contract the stored elastic energy is released simultaneously. The hips begin to extend first, followed by the knee and then the ankle (Nauwelaerts et al., 2005). Once the legs are straight and the longest toe tips have left the ground, no more work can be performed on the solid ground.

Leaping from water is different than leaping from land. Water moves when a force is applied. Anuran feet have relatively large surface areas compared to other tetrapods but will slip back if the force is applied to water. Water leaping is fundamentally different than how basilisks run on water because their bodies are above the water and the feet enter the water from the air (Glasheen & McMahon, 1996; Hsieh, 2003; Hsieh & Lauder, 2004). Drag is a factor when calculating total work because water

leaping frogs have to overcome it. Another factor is an added mass of water surrounding the body that the frog must accelerate in addition to body mass. Because of the feet slipping backwards, drag, and the added mass the V_{to} should be less than leaping on land or the frog must produce more power to leave the water. *Euphlyctis cyanophlyctis* and *E. hexadactylus* are two species known to water leap. It has been shown that these species have shorter feet lengths when compared to *R. esculenta*, but other normalized morphometrics did not differ. Water leaping *Euphlyctis* hindlimb joint extension sequence was the same as *L. catesbeianus*. *Euphlyctis* was observed to have a V_{to} of $2.9 \text{ m}\cdot\text{s}^{-1}$ (Nauwelaerts et al., 2005) which was similar to *L. catesbeianus* V_{to} of $3.24 \text{ m}\cdot\text{s}^{-1}$.

Land leaping bullfrog acceleration and power outputs compared to other species of frogs and burst running lizards are comparable. Bullfrogs can attain an acceleration, which is mean V_{to} divided by the mean duration of the leap, of $43.24 \text{ m}\cdot\text{s}^{-2}$. Force could then be calculated as the mean mass of the frogs multiplied by mean acceleration. Using the ballistics formula for distance equals V_{to}^2 divided by gravitational acceleration. Once the distance was known, multiplying force by distance yielded work. Power is calculated as the rate of work and was $147.8 \text{ W}\cdot\text{kg}^{-1}$ at a 45° take-off angle. Adult *Limnodynastes peronii*, smaller frogs $\sim 0.02 \text{ kg}$ compared to the bullfrogs I studied, were calculated to have mean acceleration of $53.3 \text{ m}\cdot\text{s}^{-2}$ and mean power output of $\sim 200 \text{ W}\cdot\text{kg}^{-1}$ at a 45° take-off angle (Wilson et al. 2000). A lizard with similar mass, *Dipsosaurus dorsalis*, at $0.026 \pm 0.056 \text{ kg}$ produced $153.7 \text{ W}\cdot\text{kg}^{-1}$ in a single stride at 40°C , which is the lizard's preferred temperature (Swoap et al. 1993). Although morphometrics in anurans is highly conserved, the elastic recoil energy storage mechanisms seen in anurans may exist in other animals to produce ballistic locomotion.

The propulsion joint extension sequence did not differ in either leaping mode. In swimming *R. esculenta*, the hip, knee, and ankle start to extend simultaneously during propulsion (Nauwelaerts et al. 2005), which suggests water leaping is less like swimming.

The difference in V_{to} for both leaps was not significant. For a water leaping frog, a slower velocity may not allow the frog to generate enough kinetic energy to overcome drag or break surface tension. If the V_{to} and overall work from the hindlimbs is not different between the two leaping modes, but water is moved, then the power output for the hindlimbs must be higher. The hindlimb joint propulsion duration for the water leap totaled ~60% of the land leap duration, which indicates that the average power output for the muscle-tendon-bone units was nearly twice as high.

The difference in the frogs' propulsive kinetic energy at $L_{straighten}$ in both leaps was not significant ($P = 0.638$). During the water leap, enough kinetic energy is obtained to leap a similar distance as during a land leap, if the take-off angle is the same. If this amount of kinetic energy is required to escape predators and capture prey on land, then it stands to reason that the same will be true for the water leap.

The transfer of KE during propulsion from the feet to the two elliptical vortex rings was only 7.3 percent. These data were obtained by a planar DPIV system I assembled that was economically designed to visualize vortex rings shed from the frog feet. A vortex ring is symmetrical and this planar DPIV system is good enough for measuring the core diameter and radius.

The parts for the DPIV system were not difficult to obtain, and most were reasonably priced. The household aquarium was a large enough to avoid boundary

effects. The aquarium tubing was inexpensive but flexible, and in concert with the compressible air in the syringes, constituted sources of error because of energy lost to those materials. The Pliolite particles were used due to their high reflectivity, animal compatibility, similarity to the density of water, and ease in altering the particle diameter. This DPIV system was economic because I adapted relatively high-powered laser-pointers as the illumination source. The economical benchtop power supply was more than enough to power the lasers. The higher-priced Phantom high-speed camera, which was priced at \$5000, was more than sufficient to perform DPIV due to its frame rate and digital image storage capacity. The DPIV software, PIVlab 1.3 (Thielicke & Stamhuis, 2012) was adequate and user-friendly, however identifying vortex cores and boundaries proved challenging and was prone to user error. Repeating DPIV analyses on the same videos was important in limiting user error.

A validation procedure was developed to test the DPIV system error using a vortex ring. The software measures the core diameter, radius, and maximal velocity of the vortex ring. Using the Pearson's chi-square test, the p-values showed no significant differences between expected volume and velocity results to measured ones.

Using biplanar high-speed videography, digitization programs, and DPIV an analysis of water leaping was made in terms of kinematics and kinetics. Bullfrogs have been known to have powerful hindlimbs that are good for leaping on land. These anurans have adaptations in which they can transition between land and water and vice versa, however with the analyses made here, the bullfrog is more capable of transitioning from water into air allowing for a way to catch aerial insects and avoid aquatic predators.

Analyzing the biomechanics of water leaping may help further understand how animals use transitioning from one medium to another to survive and reproduce.

References

- Astley, H. C., & Roberts, T. J. (2012). Evidence for a vertebrate catapult: elastic energy storage in the Plantaris tendon during frog leaping. *Biology Letters*, 8(3), 386-389.
- Glasheen, J. W., & McMahon, T. A. (1996). A hydrodynamic model of locomotion in the basilisk lizard. *Letters to Nature*, 380, 340-342.
- Guinet, C., & Bouvier, J. (1995). Development of intentional stranding hunting techniques in killer whale (*Orcinus orca*) calves at Crozet Archipelago. *Canadian Journal of Zoology*, 73(1), 27-33.
- Hart, C. B., & Giszter, S. F. (2004). Modular premotor drives and unit bursts as primitives for frog motor behaviors. *The Journal of Neuroscience*, 24(22), 5269-5282.
- Hart, C. B., & Giszter, S. F. (2010). A neural basis for motor primitives in the spinal cord. *The Journal of Neuroscience*, 30(4), 1322-1336.
- Hsieh, T. S. (2003). Three-dimensional hindlimb kinematics of water running in the plumed basilisk lizard (*Basiliscus plumifrons*). *The Journal of Experimental Biology*, 206, 4363-4377.
- Hsieh, T. S., & Lauder, G. V. (2004). Running on water: Three-dimensional force generation by basilisk lizards. *Proceedings of the National Academy of Sciences*, 101(48), 16784-16788.
- Nauwelaerts, S., Scholliers, J., & Aerts, P. (2004). A functional analysis of how frogs leap out of water. *Biological Journal of the Linnean Society*, 83, 413-420.
- Nauwelaerts, S., Stamhuis, E., & Aerts, P. (2005). Swimming and leaping in a semi-aquatic frog. *Animal Biology*, 55(1), 3-15.
- Swoap, S. J., Johnson, T. P., Josephson, R. K., & Bennett, A. F. (1993). Temperature, muscle power output and limitations on burst locomotor performance of the lizard *Dipsosaurus dorsalis*. *The Journal of Experimental Biology*, 174(1), 185-197.
- Thielicke, W., and E. J. Stamhuis. 2012. PIVlab - Time-Resolved Digital Particle Image Velocimetry Tool for MATLAB. Ver. 1.32
- Whitfield A.K. and Blaber S.J.M., 1978. Feeding ecology of piscivorous birds at Lake St Lucia, part 1: diving birds. *Ostrich*, 49, 185-198.
- Wilson, R. S., Franklin, C. E., & James, R. S. (2000). Allometric scaling relationships of jumping performance in the striped marsh frog *Limnodynastes peronii*. *Journal of Experimental Biology*, 203(12), 1937-1946.

